Journal of Theoretical Biology 460 (2019) 170–183

Contents lists available at ScienceDirect

Journal of Theoretical Biology

journal homepage: www.elsevier.com/locate/jtb

Viral replication modes in single-peak fitness landscapes: A dynamical systems analysis

Joan Fornés[a], J. Tomás Lázaro[a,b], Tomás Alarcón[b,c,d,e], Santiago F. Elena[f,g], Josep Sardanyés[c,b,*]

[a] Departament de Matemàtiques, Universitat Politècnica de Catalunya, Av Diagonal, 647, Barcelona 08028, Spain
[b] Barcelona Graduate School of Mathematics (BGSMath) Campus de Bellaterra, Edifici C, Bellaterra, Barcelona 08193, Spain
[c] Centre de Recerca Matemàtica, Campus de Bellaterra, Edifici C, Bellaterra, Barcelona 08193, Spain
[d] ICREA, Pg. Lluis Companys 23, Barcelona 08010, Spain
[e] Departament de Matemàtiques, Universitat Autònoma de Barcelona, Barcelona, Spain
[f] Instituto de Biología Integrativa de Sistemas, CSIC-Universitat de València, Parc Cientific UV, Catedrático Agustín Escardino 9, Paterna, València 46980, Spain
[g] The Santa Fe Institute, 1399 Hyde Park Road, Santa Fe, NM 87501, USA

ARTICLE INFO

Article history:
Received 25 December 2017
Revised 30 August 2018
Accepted 2 October 2018
Available online 6 October 2018

Keywords:
Bifurcations
Dynamical systems
Error threshold
Replication modes
RNA viruses
Single-peak fitness landscape

ABSTRACT

Positive-sense, single-stranded RNA viruses are important pathogens infecting almost all types of organisms. Experimental evidence from distributions of mutations and from viral RNA amplification suggest that these pathogens may follow different RNA replication modes, ranging from the stamping machine replication (SMR) to the geometric replication (GR) mode. Although previous theoretical work has focused on the evolutionary dynamics of RNA viruses amplifying their genomes with different strategies, little is known in terms of the bifurcations and transitions involving the so-called error threshold (mutation-induced dominance of mutants) and lethal mutagenesis (extinction of all sequences due to mutation accumulation and demographic stochasticity). Here we analyze a dynamical system describing the intracellular amplification of viral RNA genomes evolving on a single-peak fitness landscape focusing on three cases considering neutral, deleterious, and lethal mutants. We analytically derive the critical mutation rates causing lethal mutagenesis and error threshold, governed by transcritical bifurcations that depend on parameters α (parameter introducing the mode of replication), replicative fitness of mutants (k_1), and on the spontaneous degradation rates of the sequences (ϵ). Our results relate the error catastrophe with lethal mutagenesis in a model with continuous populations of viral genomes. The former case involves dominance of the mutant sequences, while the latter, a deterministic extinction of the viral RNAs during replication due to increased mutation. For the lethal case the critical mutation rate involving lethal mutagenesis is $\mu_c = 1 - \varepsilon/\sqrt{\alpha}$. Here, the SMR involves lower critical mutation rates, being the system more robust to lethal mutagenesis replicating closer to the GR mode. This result is also found for the neutral and deleterious cases, but for these later cases lethal mutagenesis can shift to the error threshold once the replication mode surpasses a threshold given by $\sqrt{\alpha} = \epsilon/k_1$.

1. Introduction

RNA viruses are characterized as fast replicators and reaching enormous populations sizes within infected hosts. However, virus' fast replication comes with the cost of extremely high mutation rates due to the lack of correction mechanisms of their RNA-dependent RNA polymerases (RdRp) (Sanjuán et al., 2010; Sanjuán and Domingo-Calap, 2016). Indeed, mutation rates are so high that viral populations are thought to replicate close to the so-called error threshold (also named error catastrophe), beyond which it is not possible to retain genetic information as mutant genomes outcompete the mutation-free genome (Eigen, 1971). These mutation rates are orders of magnitude higher than those characteristic for their cellular hosts. While the combination of fast replication, large population size and high mutation rate create the potential for quick adaptation to new environmental conditions (*e.g.*, changes in host species or the addition of an antiviral drug), in a stable environment such a strategy has the drawback of generating a high load of deleterious mutations. Therefore, natural selection

---

* Corresponding author. Tel.: +34 93 586 8514.
E-mail address: jsardanyes@crm.cat (J. Sardanyés).

https://doi.org/10.1016/j.jtbi.2018.10.007

may have favored life history traits mitigating the accumulation of deleterious mutations.

One such life history trait that has received a good deal of attention is the mechanism of within-cell viral replication. In the continuum of possible modes of replication, the two extremes have been particularly well studied. At one extreme, the stamping machine mode (Stent, 1963), hereafter referred as SMR, implies that the first infecting genome is transcribed into a small number of molecules of opposite polarity that will then be used as templates to generate the entire progeny of genomes. At the other extreme, the geometric replication mode (Luria, 1951), hereafter named as GR, means that the newly generated progeny also serves as template to produce new opposite polarity molecules that, themselves, will also serve to generate new progeny genomes, repeating the cycle until cellular resources are exhausted and replication ends. The actual mode of replication of a given virus may lie between these two extremes. Some RNA viruses such as bacteriophages $\phi 6$ (Chao et al., 2002) and $Q\beta$ (Garcia-Villada and Drake, 2012) and turnip mosaic virus (Martínez et al., 2011) tend to replicate closer to the SMR. In contrast, for other RNA viruses such as poliovirus (Schulte et al., 2015) or vesicular stomatitis virus (Combe et al., 0000), replication involves multiple rounds of copying per cell, and thus a mode of replication that should be closer to the GR. For DNA viruses, GR is the most likely mechanism of replication given their double-stranded nature, *e.g.*, bacteriophage T2 (Luria, 1951). Exceptions maybe be single-stranded DNA viruses, such as bacteriophage $\phi X174$, that replicate via the SMR mode because it uses a rolling circle mechanism (Hutchison and Sinsheimer, 1966).

At which point of the continuum between these two extreme modes of genome replication resides a particular virus has important evolutionary consequences. Under SMR only the parental virus is used as template for the production of progeny. In this case the distribution of mutants remains purely Poisson because mutants do not replicate. The resulting Poisson distribution has the characteristic of its mean and variance being the same. On the other hand, under the GR, the mutant progeny also serves as template for additional progeny and the resulting distribution has a variance larger than mean because mutant progeny produce more mutant viruses. This particular distribution is known as the Luria–Delbrück distribution (Luria and Delbrück, 1943). For this reason, it has been suggested that the SMR model has been selectively favored in RNA viruses because it compensates for the extremely high error rate of their RdRps (Elena et al., 2006; Sardanyés and Elena, 2011; Sardanyés et al., 2009). Alternatively, having a larger variance in the number of mutant genotypes may be beneficial in terms of evolvability under fluctuating environments. However, it remains unknown whether a given virus can modify its replication mode in response to specific selective pressures to promote or down-regulate mutational output.

Despite some previous theoretical and computational results aiming to explore the implications of the different replication modes on the accumulation of mutations and possible population extinctions (Sardanyés and Elena, 2011; Sardanyés et al., 2009), the evolutionary dynamics and, especially, the bifurcations tied to both the SMR or the GR modes are not fully understood. For example, the role of the topography of the underlying fitness landscape on error thresholds and, especially, on lethal mutagenesis have not been investigated in RNA viruses with asymmetric replication modes. Lethal mutagenesis, as compared to the error threshold, is the process by which viral genotypes go extinct due to an unbearable accumulation of mutations along with stochastic effects of small effective population sizes (Bull and Wilke, 2007). Evidence for lethal mutagenesis come from *in vitro* experiments in which mutation rates were artificially increased by adding different chemical mutagens to HIV-1 (Loeb et al., 1999), lymphocytic choriomeningitis virus (Grande-Pérez et al., 2002) or influenza A virus (Pauley and Lauring, 2015). *In vivo* evidence of lethal mutagenesis have also been recently reported for tobacco mosaic virus (Díaz-Martínez et al., 2018).

Transitions in viral populations leading to extinctions or decreased viral replication capabilities could correspond to bifurcations. Bifurcations are extremely relevant phenomena since they can be useful to understand how the population dynamics of replicators behave when parameters change. Also, the nature of the bifurcations (i.e., either smooth or abrupt) can have important implications in the ecological and evolutionary dynamics of pathogens. Recently, the analysis of a dynamical system given by a model with two variables identified a transcritical bifurcation at crossing a bifurcation threshold. For this model, the bifurcation could be either achieved by tuning the parameter that adjusted for the mode of replication or by increasing the degradation rate of the strands (Sardanyés et al., 2012). However, this model only considered the amplification dynamics of both $(+)$ and $(-)$ sense RNA strands. That is, evolution was not taken into account in the model.

In this article, we sought to investigate a quasispecies-like model given by a dynamical system describing the processes of replication and mutation of viral RNA considering an asymmetry parameter to take into account different replication modes. This parameter allows us to investigate the impact of different modes of replication (either the extreme cases: purely SMR or GR, or a mixture of replication modes, see Fig. 1a). The dynamics is assumed to take place on the Swetina–Schuster single-peak fitness landscape (see Fig. 1b) (Swetina and Schuster, 1982). This landscape, albeit being an extreme oversimplification of highly rugged (Lalic and Elena, 2015) and time-varying (Lalic and Elena, 2015) fitness landscapes identified in RNA viruses, has been widely investigated (Bull and Lachmann, 2005; Pastor-Satorras and Solé, 2001; Solé et al., 2006).

The single-peak fitness landscape allows us to group together the entire mutant spectrum into an average sequence with a lower or equal fitness than the mutation-free (master) sequence, which is located at the top of the only peak in the landscape. Such a landscape allows us to consider the three different cases for the mutant sequences, given by a pool of (1) neutral, (2) deleterious and (3) lethal mutants, thus making the distance from the optimum to the base of the peak and its steepness as large as desired. Indeed, an additional well-studied property of the Swetina–Schuster landscape is the error threshold, which emerges as an inherent property of the landscape for deleterious mutations. To keep it as simple as possible, the model does not incorporate recombination as an additional source of variation. This dynamical system is investigated analytically and numerically focusing on three main parameters: mutation rates, the mode of replication, and the fitness of the mutant sequences which allow us to consider three different mutational fitness effects mentioned above.

The structure of the paper is as follows. In Section 2 we introduce the basic properties of the mathematical model that will be analysed in the following sections. The existence of non-trivial equilibrium points, that is, situations in which coexistence of mutants and master sequences may be possible as a function of the mechanism of replication are evaluated in Section 3, while their stability is analysed in Section 4. In Section 5 we describe the type of bifurcations found in the model and their properties in terms of virus dynamics. Finally, Section 6 is devoted to summarize and drawn some conclusions from the previous sections. In the Appendix Section we provide the proofs for the propositions developed in Sections 3 and 4. It is presented keeping in mind more mathematically-oriented readers but can be skipped by others without losing the main messages of the paper.

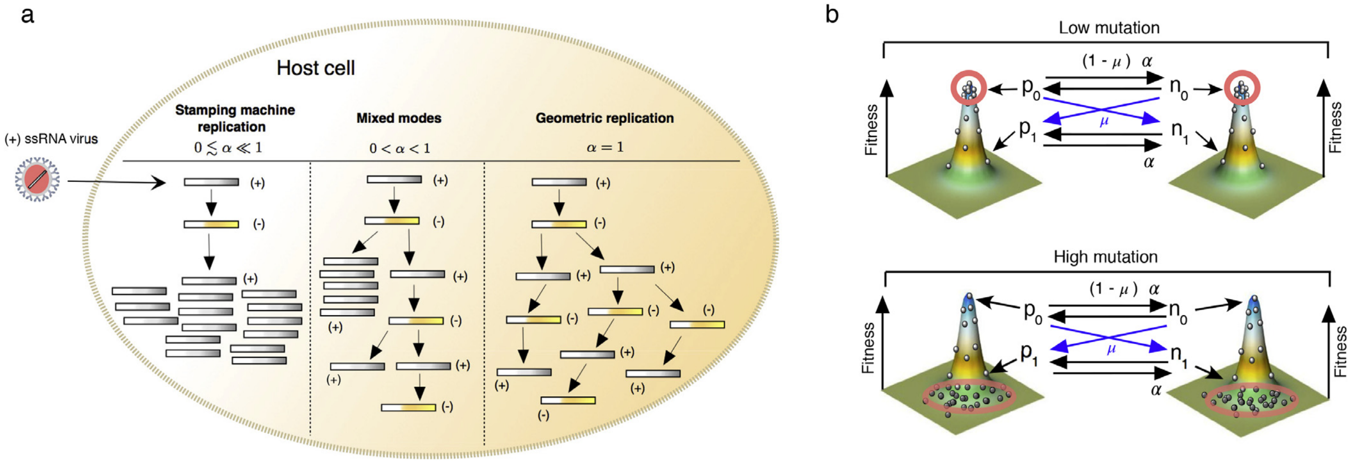

Fig. 1. (a) Schematic diagram of the processes modeled by Eqs. (1)–(4), which consider $(+)$ and $(-)$ sense viral genomes (denoted by variables p and n, respectively). Upon infection, the viral genome is released within the host cell. Such a genome can be amplified following the Stamping Machine Replication (SMR) mode, the Geometric Replication (GR) model, or mixed modes. Asymmetries in replication are introduced through parameter α (studied as $\sqrt{\alpha}$): with $0 \lesssim \alpha \ll 1$ for SMR modes; $0 < \alpha < 1$ for mixed modes; and $\alpha = 1$ for GR. Note that for SMR the offspring is produced from the $(-)$ sense template, while for GR each RNA strand is replicated with the same efficiency. (b) The model includes evolution on a Swetina–Schuster single-peak fitness landscape with master (p_0, n_0) and mutant (p_1, n_1) genomes. At low mutation, the quasispecies is located at the peak, but at high mutations the quasispecies can suffer an error catastrophe and the population falls to the valley.

2. Mathematical model

Here we introduce a minimal model describing the dynamics of symmetric and differential replication modes between $(+)$ and $(-)$ RNA viral genomes. As a difference from the model investigated in Sardanyés et al. (2009), which considered a more detailed description of the intracellular amplification kinetics, our model only considers the processes of replication and mutation, together with the degradation of RNA strands and their competition. The model considers four state variables: master and mutant classes of $(+)$ sense genome and master and mutant classes of $(-)$ sense viral genomes, labeled as p and n, respectively. Subindices 0 and 1 indicate whether we are dealing with master or mutant types, respectively (see Fig. 1). The dynamical equations are defined by:

$$\frac{dp_0}{dt} = k_0(1-\mu)n_0 \cdot \phi(\vec{p},\vec{n}) - \varepsilon_0 p_0, \tag{1}$$

$$\frac{dn_0}{dt} = \alpha k_0(1-\mu)p_0 \cdot \phi(\vec{p},\vec{n}) - \varepsilon_0 n_0, \tag{2}$$

$$\frac{dp_1}{dt} = (k_0\mu n_0 + k_1 n_1) \cdot \phi(\vec{p},\vec{n}) - \varepsilon_1 p_1, \tag{3}$$

$$\frac{dn_1}{dt} = \alpha(k_0\mu p_0 + k_1 p_1) \cdot \phi(\vec{p},\vec{n}) - \varepsilon_1 n_1. \tag{4}$$

The concentration variables or population numbers span the 4*th*-dimensional open space:

$$\mathbb{R}^4 : \{p_0, p_1, n_0, n_1; -\infty < p_i, n_i < \infty, i = 0, 1\},$$

only part of which is biologically meaningful:

$$\Pi \subset \mathbb{R}^4; \Pi : \left\{p_0, p_1, n_0, n_1;\ \ p_j, n_j \geq 0, j = 0, 1\right\}.$$

The constants $k_0 > 0$ and $k_1 \geq 0$ are the replication rates of the master and the mutant genomes, respectively. Mutation rate is denoted by $0 \leq \mu \leq 1$. Since we are studying deleterious fitness landscapes and lethality, we will set $k_0 = 1$. The term ϕ, present in all of the equations, is a logistic-like constraint, which introduces competition between the viral genomes and bounds the growth of the system (Sardanyés et al., 2012). This term is given by

$$\phi(\vec{p},\vec{n}) = 1 - K^{-1}\sum_{i=0}^{1}(p_i + n_i),$$

K being the carrying capacity (hereafter we assume $K = 1$). Parameters ε_0 and ε_1 correspond to the spontaneous degradation rates of master and mutant genomes, with $0 < \varepsilon_{0,\,1} \ll 1$. Finally, parameter α introduces the mode of replication for the RNAs (Sardanyés et al., 2012). Two extreme cases can be identified: when $\alpha = 1$, both $(+)$ and $(-)$ sense strands replicate at the same rates, following GR that results in exponential growth at low population numbers (Sardanyés et al., 2009). When $0 \lesssim \alpha \ll 1$, the contribution from $(+)$ as templates to produce $(-)$ strands is much lower, and thus the progeny of genomes is mainly synthesized from the initial $(-)$ sense templates transcribed at the beginning of the infection process, giving rise to an SMR mode. The initial replication dynamics for the SMR replication might thus follow sub-exponential growth (Sardanyés et al., 2009). Between these two extremes, our model considers a continuum of asymmetric replication modes i.e., $0 < \alpha < 1$. These dynamical behaviors are well reproduced by Eqs. (1)–(4), as shown in Fig. 2, where the different initial kinetics of the strands is displayed for several replication modes.

To simplify the exposition, we will assume the following nonrestrictive hypotheses on our model: (H1) equal degradation rates $\varepsilon_0 = \varepsilon_1 = \varepsilon$ and, as mentioned, a fixed fitness value for the master genomes, setting $k_0 = 1$; (H2) the degradation rate ε is smaller than the mutation rate, that is, $0 < \varepsilon \leq \min\{1-\mu, k_1\}$.

Our model assumes no backward mutations, that is, mutant sequences of one polarity can not give rise to master sequences of the complementary polarity. The length of RNA viral genomes (about 10^6 nucleotides) makes the probability of backward mutations to be extremely low. This is a common assumption in quasispecies models that simplifies the dynamical equations (see e.g., Bull and Lachmann, 2005; Pastor-Satorras and Solé, 2001; Solé et al., 2006).

The quasispecies studied here inhabits a single-peak fitness landscape (Swetina-Schuster; Fig. 1b). Different heights of this fitness landscape can be studied by tuning $0 \leq k_1 \leq 1$, considering different mutational fitness effects. The aim of abstract quasispecies models since conceived by Eigen in his seminal work (Eigen, 1971) was to understand the dynamics of mutation and selection of molecular replicators in a well mixed environment. It is assumed that the fitness of such replicators depends on their mutational load in a generic manner, which means that fitness is assigned according to the value of the mutations carried by a genome rather than by the effect these mutations may have on protein activity.

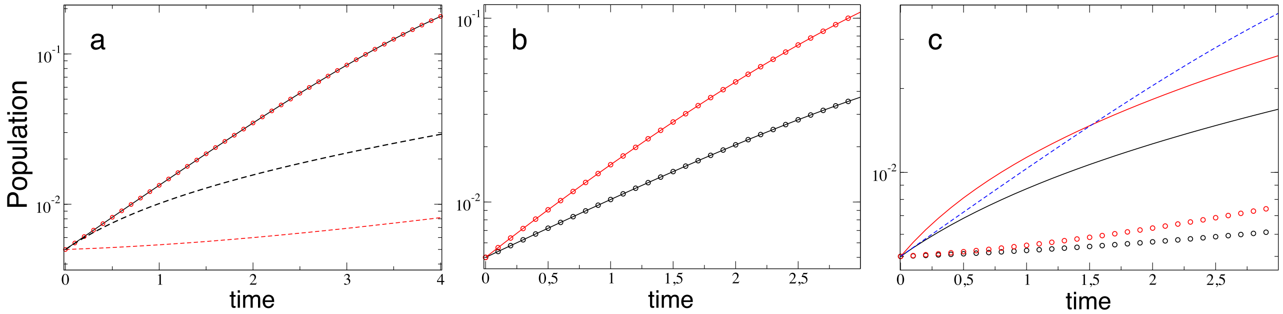

Fig. 2. (a) Strands' initial dynamics with $\mu = 0$ and $p_0(0) = n_0(0) = 0.005$. The growth for the GR mode ($\alpha = 1$) is exponential for small population sizes, resulting in a straight line in a linear-log scale: here p_0 (solid black line) and n_0 (red circles). The two curves below, which follow sub-exponential growth, correspond to the SMR with $\alpha = 0.05$: p_0 (dashed black) and n_0 (red dashed). (b-c) Initial amplification phase with $\mu = 0.25$ and $p_{0,1}(0) = n_{0,1}(0) = 0.005$. In (b) we show the dynamics for GR with $\alpha = 1$: p_0 (black solid); p_1 (black circles); n_0 (red solid); and n_1 (red circles). In (c) we display the same results of (b) but considering SMR with $\alpha = 0.05$. For comparison, the blue dashed line corresponds to the growth of p_0 with $\alpha = 1$ shown in (b), which results in a straight line. In all panels we set: $k_{0,1} = 1$ and $\varepsilon_{0,1} = 10^{-5}$. (For interpretation of the references to color in this figure legend, the reader is referred to the web version of this article.)

From a real-life virology perspective, this is an extreme simplification as the fitness of the virus would depend on the activity and interactions of encoded proteins, the ability of the virus to spread and infect other cells and, finally, be transmitted among individuals. However, for the sake of simplicity, hereafter we follow Eigen's approach and refer to fitness as a property of the molecular replicators. In general terms, mutations can be deleterious, neutral, lethal, or beneficial for the replicators in their intracellular environment. Some quantitative descriptions of the fitness effects of mutations reveal that about 40% of mutations are lethal, and about 20% are either deleterious or neutral. For the within-cell replication time-scale, beneficial mutations were produced with a very low percentage i.e., about 4% (see Carrasco et al., 2007; Sanjuán et al., 2004 and references therein). Specifically, in our model we will distinguish three different cases:

1. *Neutral mutants* ($k_0 = k_1 = 1$). Mutations are neutral and thus mutant genomes have the same fitness than the master ones.
2. *Deleterious mutants* ($0 \lesssim k_1 < k_0 = 1$). This case corresponds to the classical single-peak fitness landscape (see Fig. 1b), where mutations are deleterious and thus the quasispecies can be separated into two classes: the master genome and an average sequence containing all mutant sequences with lower fitness.
3. *Lethal mutants* ($k_1 = 0$). For this case, mutations are assumed to produce non-viable, lethal genotypes which can not replicate.

At this point, we want to emphasise that our model is only considering different viral genotypes with different kinetic properties since we are interested in the impact of differential RNA amplification in simple fitness landscapes. This is why fitness is introduced as genomes' replication speed. Our model could be used to introduce further complexity in terms of fitness landscapes and/or in terms of the within-cell infection dynamics, following the spirit of Ref. Sardanyés et al. (2009).

3. Equilibrium states

In this section we first compute the equilibrium points of Eqs. (1)–(4) and characterize their existence conditions. That is, under which parameter values the fixed points live at the boundaries or inside the phase space Π. Let us define the following constants, which will appear in the equilibrium states (see Proposition 1) and also in their stability discussion

$$\nu_0 := \frac{\varepsilon}{1-\mu}, \qquad \nu_1 := \frac{\varepsilon}{k_1}, \qquad c_\alpha := \frac{1}{\sqrt{\alpha}(1+\sqrt{\alpha})}, \tag{5}$$

and

$$\delta := \frac{\mu\nu_0}{k_1(\nu_1-\nu_0)}, \qquad \delta^0 := \frac{\mu\nu_0}{\varepsilon}. \tag{6}$$

From these definitions, one has the equivalences:

$$k_1 < (1-\mu) \iff \nu_0 < \nu_1, \tag{7}$$

$$k_1 = (1-\mu) \iff \nu_0 = \nu_1 = \nu, \tag{8}$$

$$k_1 > (1-\mu) \iff \nu_1 < \nu_0. \tag{9}$$

Moreover hypothesis (H2) implies that $0 < \nu_0 \le 1$ and $0 < \nu_1 \le 1$.

Proposition 1. *System (1)–(4) presents the following equilibria:*

1. *In the Deleterious* ($0 < k_1 < 1$) *and neutral* ($k_1 = 1$) *cases, there are three possible equilibrium points:*
    - *Total extinction: the origin,* $\mathcal{O} = (0, 0, 0, 0)$.
    - *Master sequences' extinction: if* $\sqrt{\alpha} > \nu_1$ *one has the point* $\mathcal{P}_1 = p_1^*(0, 0, 1, \sqrt{\alpha})$, *where* $p_1^* = c_\alpha(\sqrt{\alpha} - \nu_1)$.
    - *Coexistence of genomes: if* $\sqrt{\alpha} > \nu_0$ *and* $\nu_0 < \nu_1$, *we have* $\mathcal{P}_2 = q_0\big(1, \sqrt{\alpha}, \delta, \delta\sqrt{\alpha}\big)$, *where* $q_0 = \dfrac{c_\alpha(\sqrt{\alpha} - \nu_0)}{1+\delta}$.
2. *Lethal case* ($k_1 = 0$). *We have two equilibrium states:*
    - *Total extinction: the origin,* $\mathcal{O} = (0, 0, 0, 0)$.
    - *Coexistence of genomes: if* $\sqrt{\alpha} > \nu_0$ *we have the point* $\mathcal{P}_2^0 = q_0^0\big(1, \sqrt{\alpha}, \delta^0, \delta^0\sqrt{\alpha}\big)$ *where* $q_0^0 = \dfrac{c_\alpha(\sqrt{\alpha} - \nu_0)}{1+\delta^0}$.

Note that for the lethal case no equilibrium state corresponding to an error threshold is found, and only lethal mutagenesis is the alternative state to the persistence of all sequences. Fig. 3 displays a diagram with the existence of the different equilibria in terms of the values of $\sqrt{\alpha}$ and the parameters ν_0, ν_1. The emergence of the non-trivial fixed points $\mathcal{P}_1, \mathcal{P}_2$ and $\mathcal{P}_2^0$ as a function of $\sqrt{\alpha}$ illustrates the transcritical bifurcations identified in the system (see Section 4 below).

Remark 1. The coexistence points $\mathcal{P}_2$ and $\mathcal{P}_2^0$ are located on straight lines passing through the origin and director vectors $(1, \sqrt{\alpha}, \delta, \delta\sqrt{\alpha})$ and $(1, \sqrt{\alpha}, \delta^0, \delta^0\sqrt{\alpha})$.

In the case $\mu = 1$, there are no master sequences $p_0 \leftrightarrow n_0$, since all master sequences mutate with probability 1. For this case, the equilibria are:

Proposition 2. *If* $\mu = 1$, *system (1)–(4) presents the following equilibria:*

1. *In the deleterious and neutral cases: the origin* $\mathcal{O}$ *(for any value of* $\sqrt{\alpha} \in [0, 1]$*) and the point* $\mathcal{P}_1$ *given at the Proposition 1 provided* $\sqrt{\alpha} > \nu_1$.

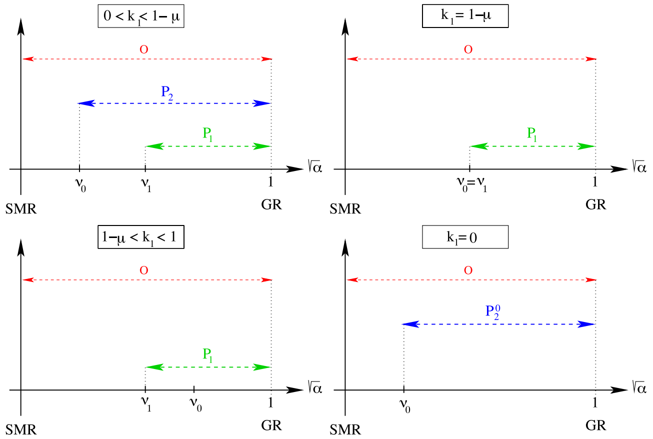

Fig. 3. Existence of equilibria in four different scenarios: (deleterious and neutral) $0 < k_1 < 1-\mu$, $k_1 = 1-\mu$, $k_1 \geq 1-\mu$ and (lethal) $k_1 = 0$, respectively. The result are displayed increasing $\sqrt{\alpha}$ from the SMR model, with $0 \lesssim \sqrt{\alpha} \ll 1$) to the GR, with $\sqrt{\alpha} = 1$) models. Here $\nu_0 = \varepsilon/(1-\mu)$ and $\nu_1 = \varepsilon/k$. Note that *y*-axes do not contain any information.

2. *In the lethal case, the unique equilibrium is the origin* $\mathcal{O}$, *for any value of* $\sqrt{\alpha} \in [0, 1]$.

Fig. 4 displays time series achieving the equilibrium points previously described. For low mutation rates, both (+) and (−) sense strands persist, and thus $\mathcal{P}_2$ is stable (Fig. 4a). Note that close to the SMR the relative frequency of (+) and (−) strands is asymmetric, as expected, while for GR both polarities achieve similar population values at equilibrium (see also Fig. 2). The increase in mutation rates can involve crossing over the error thresholds (since $\mathcal{P}_1$ becomes stable), and the quasispecies is dominated by the mu-

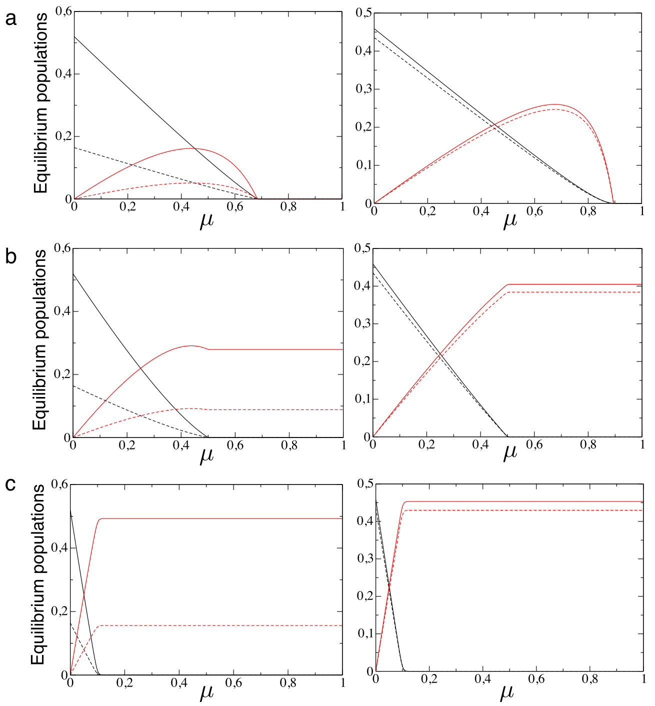

Fig. 5. Equilibrium populations at increasing mutation rate μ, with $\alpha = 0.1$ (first column) and $\alpha = 0.9$ (second column). We analyse three different cases with: $k_1 = 0.1$ (a); $k_1 = 0.5$ (b); and $k_1 = 0.9$ (c). In all of the panels we have set $\varepsilon = 0.1$ and the initial condition $(p_0(0), n_0(0), p_1(0), n_1(0)) = (0.1, 0, 0, 0)$. Here, as in Fig. 4: (+) sense master (solid black line); (+) sense mutant (solid red line); (−) sense master (dashed black line); and (−) sense mutant (dashed red line). (For interpretation of the references to color in this figure legend, the reader is referred to the web version of this article.)

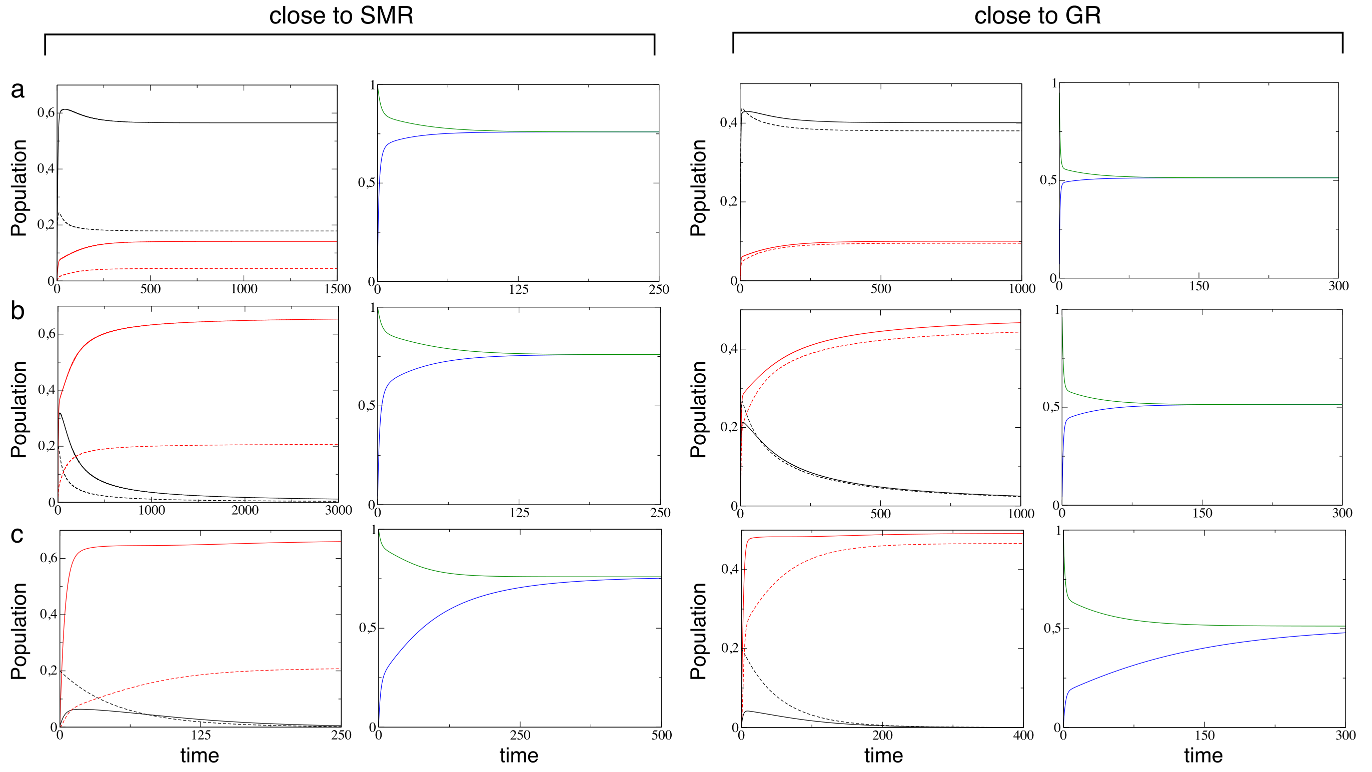

Fig. 4. Time series for positive (solid lines) and negative (dashed lines) sense sequences close to the SMR (with $\alpha = 0.1$) and close to the GR (with $\alpha = 0.9$) modes. Here master and mutant sequences are represented in black and red, respectively. For each mode of replication: (a) $k_1 < (1-\mu)$ with $\mu = 0.1$; (b) $k_1 = (1-\mu)$ with $\mu = 0.5$ and (c) $k_1 > (1-\mu)$ with $\mu = 0.9$. In all of the panels we have set $k_1 = 0.5$, $\varepsilon = 0.02$. We also display the time series gathering the variables as follows: $p_0(t)/(n_0(t) + p_0(t))$ (green); and $p_1(t)/(n_1(t) + p_1(t))$ (blue). (For interpretation of the references to color in this figure legend, the reader is referred to the web version of this article.)

tant sequences (Fig. 4b with $\alpha = 0.1$ and Fig. 4c for $\alpha = 0.1$ and $\alpha = 0.9$). The relative population of master (green) and mutant (blue) (+) sense sequences is displayed in the second and fourth columns of Fig. 4. Here also the relative frequencies of p_0 and p_1 achieve values close to 0.5 for the GR model, indicating that the production of both strands polarities occurs at similar rates.

Fig. 5 displays the equilibrium populations of the four state variables at increasing mutation rates computed numerically. These results illustrate the scenarios of lethal mutagenesis (all-sequences extinction) and error threshold (outcompetition of the master sequence by the mutants). The first column displays the results for a replication mode close to the SMR ($\alpha = 0.1$) while the second one displays the same results for $\alpha = 0.9$, a case closer to the GR model. When the fitness of the mutants is low, the SMR is less robust to lethal mutagenesis at increasing mutation. Extinction of the master sequences under GR takes place at higher mutation rates (see Fig. 5a). For those cases with higher fitness for mutants (Fig. 5b,c), the full extinction of genomes is replaced by an error threshold, since there exists a critical value of μ involving the dominance of the mutant genomes and the extinction of the master sequences. Hence, this figure indicates that the shift from lethal mutagenesis to error threshold mainly depends on the fitness of sequences, and that the mode of replication has the strongest impact on low-fitness mutants, driving to lethal mutagenesis.

In the following sections we generalize the results displayed in Figs. 4–6 by means of a deep analysis of the stability and the bifurcations of Eqs. (1)–(4).

4. Local stability of the equilibria

After determining the equilibrium points, our next step is to evaluate their stability to small variations in the model parameters. An stable equilibrium would mean that the viral population composed by master and mutants of both polarities is robust to external perturbations whereas an unstable equilibrium would mean that the viral population will rapidly change in response to perturbations without returning to the equilibrium. This section is devoted to the study of the linear (and also in the majority of cases of the nonlinear) stability of the equilibria found in the previous section. We will consider separately the three equilibrium points $\mathcal{O}$, $\mathcal{P}_1$ and $\mathcal{P}_2$. As it is standard, it will be performed by considering the linearized system around the three equilibrium points. Particular attention will be given to the change of stability of the equilibrium points that can indicate the presence of bifurcations, which are investigated in Section 5. From now on we denote by F the vector field related to our system given by Eqs. (1)–(4).

4.1. Stability of the origin

Proposition 3. *Let us consider the constants ν_0, ν_1, c_α defined in (5). Then, the jacobian matrix at the origin $DF(\mathcal{O})$ has the following eigenvalues:*

$$\begin{aligned}\lambda_1 &= -\varepsilon + \sqrt{\alpha}(1-\mu),\\ \lambda_2 &= -\varepsilon - \sqrt{\alpha}(1-\mu),\\ \lambda_3 &= -\varepsilon + k_1\sqrt{\alpha},\\ \lambda_4 &= -\varepsilon - k_1\sqrt{\alpha}.\end{aligned}$$

Observe that all of them are real and that λ_2, λ_4 are always negative since $0 < \mu < 1$ and $k_1 \geq 0$. This means that the linear (and local nonlinear) stability of the origin will be determined by the signs of λ_1 and λ_3. Let us consider the following two cases:

1. *Deleterious and neutral case ($0 < k_1 \leq 1$): the three following scenarios hold:*
   - (i) *If $k_1 < 1 - \mu$ or, equivalently, $\nu_0 < \nu_1$: The origin $\mathcal{O}$ is locally asymptotically stable (a sink) for $\sqrt{\alpha} < \nu_0$ and unstable for $\sqrt{\alpha} > \nu_0$. For $\sqrt{\alpha} = \nu_0$ we have the birth of $\mathcal{P}_2$. More precisely, if $\nu_0 < \sqrt{\alpha} < \nu_1$ then $\dim W^u_{\mathrm{loc}}(\mathcal{O}) = 1$ and if $\sqrt{\alpha} > \nu_1$ then $\dim W^u_{\mathrm{loc}}(\mathcal{O}) = 2$, where $W^u_{\mathrm{loc}}(\mathcal{O})$ denotes the local unstable invariant manifold of the equilibrium point $\mathcal{O}$.*
   - (ii) *If $k_1 = 1 - \mu$ or, equivalently, $\nu_0 = \nu_1 = \nu$: In this situation, $\mathcal{O}$ is locally asymptotically stable (a sink) for $\sqrt{\alpha} < \nu$ and unstable for $\sqrt{\alpha} > \nu$. This change in its stability coincides with the birth of $\mathcal{P}_1$. Recall that if $\nu_0 = \nu_1$ the point $\mathcal{P}_2$ does not exist. Moreover, when crossing the value $\sqrt{\alpha} = \nu$ one has that $\dim W^u_{\mathrm{loc}}(\mathcal{O})$ passes from 0 to 2.*
   - (iii) *If $k_1 > 1 - \mu$ or, equivalently, $\nu_1 < \nu_0$: Again, the origin is locally asymptotically stable (a sink) for $\sqrt{\alpha} < \nu_1$ and unstable for $\sqrt{\alpha} > \nu_1$, coinciding with the birth of the equilibrium point $\mathcal{P}_1$. As in the precedent case, no point $\mathcal{P}_2$ exists. As above, if $\nu_1 < \sqrt{\alpha} < \nu_0$ then $\dim W^u_{\mathrm{loc}}(\mathcal{O}) = 1$ and if $\sqrt{\alpha} > \nu_0$ then $\dim W^u_{\mathrm{loc}}(\mathcal{O}) = 2$,*
2. *Lethal case ($k_1 = 0$): Taking into account again Proposition 1, the origin $\mathcal{O}$ changes its stability from locally asymptotically stable (a sink) to unstable (a saddle) when $\sqrt{\alpha}$ crosses ν_0. As above, this coincides with the birth of $\mathcal{P}_2$.*

Cases (i)–(iii) are displayed in Fig. 6a–c, respectively. Specifically, the local stability of the origin for each case is shown as a function of $\sqrt{\alpha}$: the upper panels in Fig. 6 display how the origin becomes unstable as the replication model changes from SMR to mixed modes. This means that under SMR the sequences are more prone to extinction, as suggested in Sardanyés et al. (2012). These stability diagrams are also represented by means of the eigenvalues λ_1, .., λ_4. The phase portraits display the orbits in the subspace (p_1, n_1). Note that the label of each phase portrait corresponds to the letters in the upper panels. Panels a.1, b.1, and c.1 show results when the origin is a global attractor. Panels a.2 and a.3 display the orbits when the origin is unstable and the stable fixed point is $\mathcal{P}_2$, where the four genomes coexist. Finally, panels b.2, c.2, b.3, and c.3 display examples of a full dominance of the mutant genomes. For these latter examples, the increase of $\sqrt{\alpha}$ involves the change from the full extinction to survival of the mutant sequences. Biologically, this means that at very high mutation rates, SMR can be driven to extinction whereas GR maintains a population replicating into the error catastrophe regime (i.e., no more master sequences exist).

4.2. Stability of the point $\mathcal{P}_1$

Proposition 4. *Let us assume $\sqrt{\alpha} > \nu_1$, in order that the equilibrium point $\mathcal{P}_1$ exists. Then, the eigenvalues of the jacobian matrix $DF(\mathcal{P}_1)$ are all real and they are given by*

$$\begin{aligned}\lambda_1 &= -\varepsilon + (1-\mu)\nu_1,\\ \lambda_2 &= -\varepsilon - (1-\mu)\nu_1,\\ \lambda_3 &= -2\varepsilon,\\ \lambda_4 &= \varepsilon - k_1\sqrt{\alpha}.\end{aligned}$$

The eigenvalues λ_2 and λ_3 are always negative. $\lambda_4 < 0$ since $\sqrt{\alpha} > \nu_1 = \varepsilon/k_1$. Having in mind that $\nu_0 = \varepsilon/(1-\mu)$, it is easy to check that:

$$\begin{aligned}\lambda_1 < 0 &\quad \text{if and only if} \quad \nu_1 < \nu_0,\\ \lambda_1 = 0 &\quad \text{if and only if} \quad \nu_1 = \nu_0,\\ \lambda_1 > 0 &\quad \text{if and only if} \quad \nu_1 > \nu_0.\end{aligned}$$

Therefore, in the deleterious-neutral case we have the following subcases:

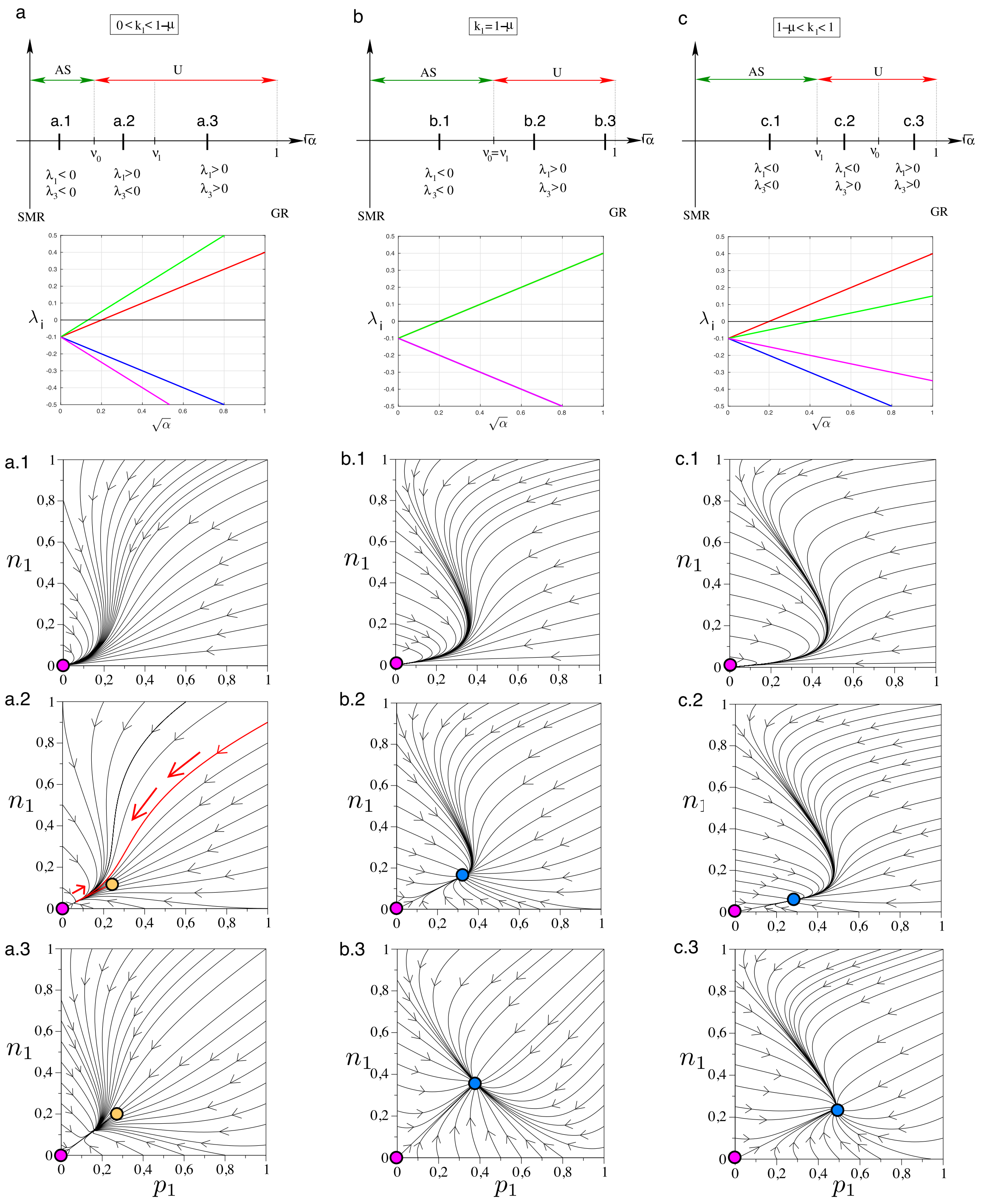

Fig. 6. Local stability of the origin $\mathcal{O}$ in three different scenarios: (a) $0 < k_1 < 1-\mu$; (b) $k_1 = 1-\mu$; (c) $k_1 \geq 1-\mu$ (AS means “asymptotically stable”; U denotes “unstable” and in all these cases means saddle type). Below each case we plot the eigenvalues of $DF(\mathcal{O})$ increasing $\sqrt{\alpha}$ with $\mu = 0.5$, $\epsilon = 0.1$, and: $k_1 = 0.25$ (a); $k_1 = 0.5$ (b); and $k_1 = 0.75$ (c). Here λ_1 (red), λ_2 (blue), λ_3 (green), and λ_4 (magenta). Phase portraits projected in the subspace (p_1, n_1) of the phase space Π are displayed setting $\mu = 0.6$, $\epsilon = 0.1$, and $k_1 = 0.15$ (a), $k_1 = 0.4$ (b), and $k_1 = 0.75$ (c). Each panel corresponds to a value of $\sqrt{\alpha}$: 0.15 (a.1); 0.25 (a.2); 0.75 (a.3); 0.15 (b.1); 0.5 (b.2); 0.95 (b.3); 0.09 (c.1); 0.2 (c.2); 0.5 (c.3). Fixed points: $\mathcal{O}$ (magenta); $\mathcal{P}_1$ (blue); $\mathcal{P}_2$ (orange). The red orbit in panel a.2 shows a trajectory that approaches the origin $\mathcal{O}$ but then returns to $\mathcal{P}2$. (For interpretation of the references to color in this figure legend, the reader is referred to the web version of this article.)

(i) *If* $k_1 < 1-\mu$ *or, equivalently,* $\nu_0 < \nu_1$*:* $\mathcal{P}_1$ *is unstable (saddle). Indeed,* $\dim W^s_{\text{loc}}(\mathcal{P}_1) = 3$ *and* $\dim W^u_{\text{loc}}(\mathcal{P}_1) = 1$, *where* $W^{s,u}_{\text{loc}}(\mathcal{P}_1)$ *denote the stable* (W^s) *and unstable* (W^u) *local invariant manifolds of* $\mathcal{P}_1$.

(ii) *If* $k_1 = 1-\mu$ *or, equivalently,* $\nu_0 = \nu_1 = \nu$*:* $\mathcal{P}_1$ *has a 1-dimensional neutral direction (tangent to the eigenvector associated to the eigenvalue* $\lambda_1 = 0$*) and a 3-dimensional local stable manifold.*

(iii) *If* $k_1 > 1-\mu$ *or, equivalently,* $\nu_1 < \nu_0$*: In this case* $\mathcal{P}_1$ *is a sink so, therefore, a local attractor.*

Regarding the lethal case ($k_1 = 0$)*, the eigenvalue* $\lambda_4 = \varepsilon$ *is always positive and so* $\mathcal{P}_1$ *is unstable (saddle).*

The proof follows from straightforward computations.

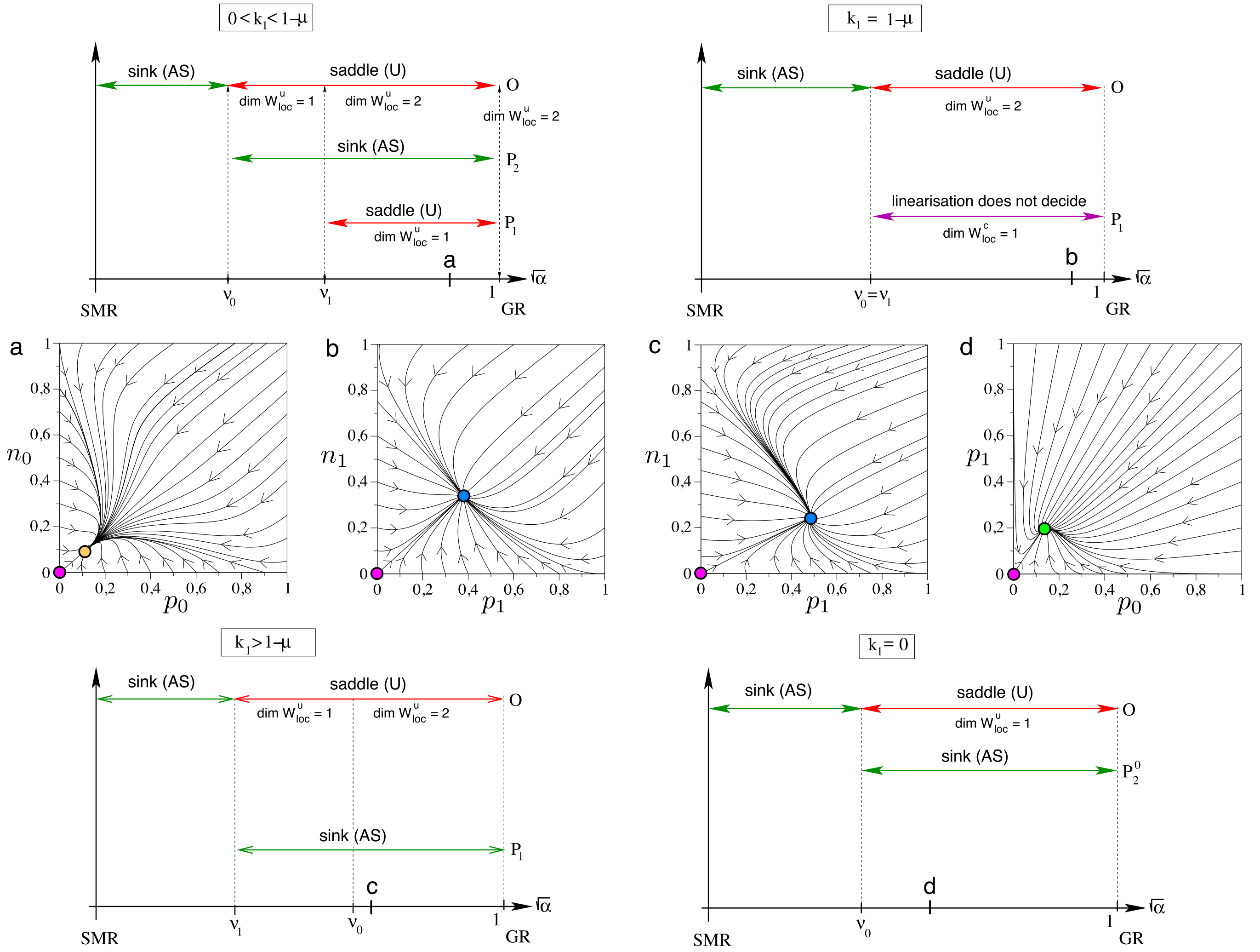

Fig. 7. Bifurcations of the equilibrium points $\mathcal{O}, \mathcal{P}_1, \mathcal{P}_2$ (deleterious-neutral cases) and $\mathcal{P}_2^0$ (lethal case). From top to bottom and left to right: deleterious-neutral case, (i) $0 < k_1 < 1 - \mu$, (ii) $k_1 = 1 - \mu$, (iii) $k_1 > 1 - \mu$; and (iv) lethal case. The phase portraits correspond to the parameter values indicated with the letters in the bifurcation diagrams with: k_1 and $\sqrt{\alpha} = 0.85$ (a); $k_1 = 0.4$ and $\sqrt{\alpha} = 0.5$ (b); $k_1 = 0.75$ and $\sqrt{\alpha} = 0.5$; and $k_1 = 0$, $\sqrt{\alpha} = 0.5$ (b). Initial conditions: $p_1(0) = n_1(0) = 0$ (a); $p_0(0) = n_0(0) = 0.1$ (b); and $p_0(0) = n_0(0) = 0$ (c–d). In all of the panels we use $\mu = 0.6$ and $\varepsilon = 0.1$. Fixed points: $\mathcal{O}$ (magenta); $\mathcal{P}_1$ (blue); $\mathcal{P}_2$ (orange); $\mathcal{P}_2^0$ (green). (For interpretation of the references to color in this figure legend, the reader is referred to the web version of this article.)

4.3. Stability of the points $\mathcal{P}_2$ and $\mathcal{P}_2^0$

From Section 3 we know that the equilibrium point $\mathcal{P}_2$ exists if $\sqrt{\alpha} > \nu_0$ and in the following two cases:

1. In the deleterious case $(0 < k_1 < 1)$ provided that $0 < k_1 < 1 - \mu$ (or, equivalently, $\nu_0 < \nu_1$).
2. In the lethal case $(k_1 = 0)$.

Next proposition determines the local stability of $\mathcal{P}_2$ in these two situations.

Proposition 5. *Let us assume that $\sqrt{\alpha} > \nu_0$ in order $\mathcal{P}_2$ and $\mathcal{P}_2^0$ to exist. Then, the eigenvalues of the differential $DF(\mathcal{P}_2)$ and $DF(\mathcal{P}_2^0)$ are, respectively:*

1. *In the deleterious case $(0 < k_1 < 1)$ provided that $0 < k_1 < 1 - \mu$ (or, equivalently, $\nu_0 < \nu_1$):*

$$\lambda_1 = -2\varepsilon, \qquad \lambda_2 = -\varepsilon - k_1\nu_0,$$

$$\lambda_\pm = -\frac{1}{2(1-\mu)}(A \pm |A - 2((1-\mu) - k_1)\varepsilon|),$$

where $A = \sqrt{\alpha}(1-\mu)^2 - k_1\varepsilon$. Notice that assumptions $\sqrt{\alpha} > \nu_0$ and $0 < k_1 < 1 - \mu$ imply that $A > 0$.

2. *In the lethal case $(k_1 = 0)$:*

$$\lambda_1 = -2\varepsilon,$$
$$\lambda_2 = -\varepsilon,$$
$$\lambda_\pm = -\frac{(1-\mu)}{2}\sqrt{\alpha} \pm \left|\frac{(1-\mu)}{2}\sqrt{\alpha} - \varepsilon\right|.$$

Then, in both cases all four eigenvalues are real and negative, and so the equilibrium points $\mathcal{P}_2$ and $\mathcal{P}_2^0$ are sinks for any $\sqrt{\alpha} > \nu_0$.

5. Bifurcations

As mentioned, the identification of the bifurcations as well as their nature (whether they are smooth or catastrophic) is important to understand how viral sequences can enter into either error threshold or lethal mutagenesis states. Essentially, the system under investigation only experiences transcritical bifurcations. This means that the collapse of the viral sequences or their entry into error threshold is governed by smooth transitions. These bifurcations coincide with the appearance of a new equilibrium point, $\mathcal{P}_1$, $\mathcal{P}_2$ or $\mathcal{P}_2^0$. It is remarkable that the latter equilibria, once becoming

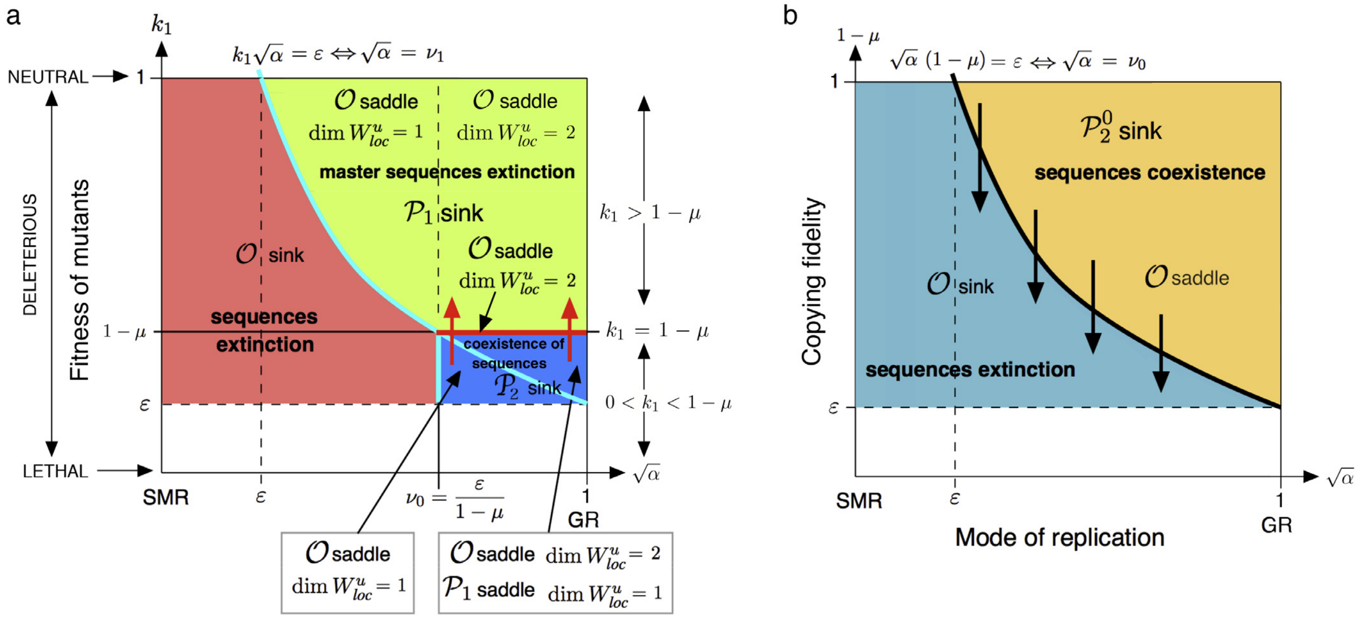

Fig. 8. Two-dimensional parameter spaces displaying the stability of the fixed points. (a) $(\sqrt{\alpha}, k_1)$-plane bifurcation diagram for the deleterious-neutral cases. The thick red line indicates the boundary for the full dominance of the mutant sequences as a function of k_1. Crossing this boundary (vertical red arrows) causes the extinction of the master sequences p_0, n_0 and the dominance of the pool of mutants (green surface). Below this line all genomes coexist (blue area). (b) $(\sqrt{\alpha}, 1-\mu)$-plane bifurcation diagram indicating the stability of the fixed points for the lethal case. The vertical black lines indicate the entry into lethal mutagenesis, where full extinctions occur (light blue). The region with survival of all sequences is colored in orange. (For interpretation of the references to color in this figure legend, the reader is referred to the web version of this article.)

an interior fixed point, remain a sink, without undergoing any bifurcation. Let us detail them in all our cases. Namely,

1. Deleteterious-neutral case ($0 < k_1 \leq 1$):
   (i) Case $0 < k_1 < 1-\mu$ (that is, $\nu_0 < \nu_1$): the origin $\mathcal{O}$ is a sink up to $\sqrt{\alpha} = \nu_0$. At that point, the equilibrium point $\mathcal{P}_2$ appears. Then, $\mathcal{O}$ changes its stability by means of a transcritical bifurcation, becomes a saddle point (unstable), with $\dim W^u_{\text{loc}}(O) = 1$. The coexistence equilibrium point $\mathcal{P}_2$ is a sink (i.e., an attractor) for $\sqrt{\alpha} \in (\nu_0, 1]$. At $\sqrt{\alpha} = \nu_1$, the equilibrium point $\mathcal{P}_1$ appears. It will be a saddle point (with $\dim W^u_{\text{loc}}(\mathcal{P}_1) = 1$) for $\sqrt{\alpha} \in (\nu_1, 1]$. At this point, $\sqrt{\alpha} = \nu_1$, the dimension of $W^u_{\text{loc}}(O)$ increases to 2, remaining like this up to $\sqrt{\alpha} = 1$.
   (ii) Case $k_1 = 1-\mu$ (that is, $\nu_0 = \nu_1$): in this situation there are only two equilibrium points, $\mathcal{O}$ and $\mathcal{P}_1$, the latter appearing at $\sqrt{\alpha} = \nu_0 = \nu_1$. As above, the origin $\mathcal{O}$ is a sink up to $\sqrt{\alpha} = \nu_0$. With the appearing of $\mathcal{P}_1$ it undergoes a transcritical bifurcation, becoming a saddle point with $\dim W^u_{\text{loc}}(O) = 2$. Concerning the point $\mathcal{P}_1$, linearisation criteria do not decide its nonlinear local stability since it has (linear) centre and stable local invariant manifolds of dimension 1 and 3, respectively. No others bifurcations show up.
   (iii) Case $k_1 > 1-\mu$ (that is, $\nu_1 < \nu_0$): similarly to the precedent cases, the origin is a sink (an attractor) until the appearance of the equilibrium $\mathcal{P}_1$ at $\sqrt{\alpha} = \nu_1$. At this point, $\mathcal{O}$ becomes unstable, a saddle with $\dim W^u_{\text{loc}}(O) = 1$. Later on, at $\sqrt{\alpha} = \nu_1$, the dimension of $W^u_{\text{loc}}(O)$ increases to 2, keeping this dimension until $\sqrt{\alpha} = 1$. No bifurcations undergone by the point $\mathcal{P}_1$, which is a sink for $\sqrt{\alpha} \in (\nu_0, 1]$.
2. Lethal case ($k_1 = 0$): there are only two equilibria: the origin $\mathcal{O}$ and the coexistence point $\mathcal{P}^0_2$, this latter appearing at $\sqrt{\alpha} = \nu_0$. The origin is a sink for $\sqrt{\alpha} \in (0, \nu_0)$, undergoes a transcritical bifurcation at $\sqrt{\alpha} = \nu_0$, becoming unstable (saddle point) with $\dim W^u_{\text{loc}}(O) = 1$. The point $\mathcal{P}^0_2$ is always a sink.

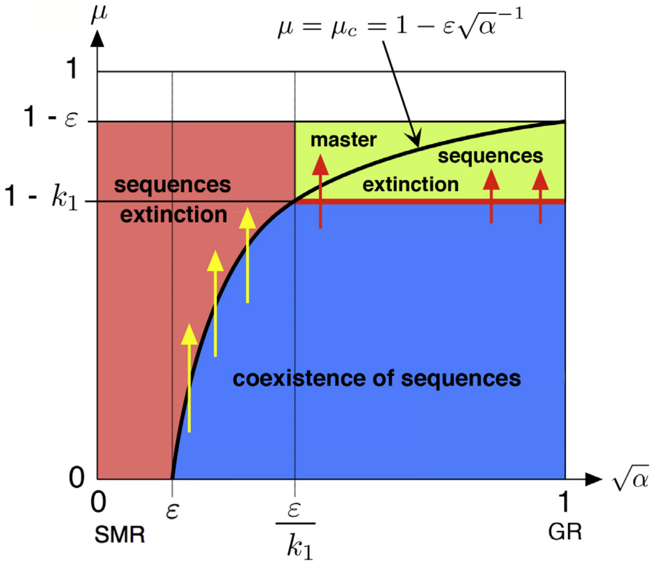

Fig. 9. Phase diagrams for the deleterious-neutral case computed numerically in the parameter space $(\sqrt{\alpha}, \mu)$. The equilibrium state is represented using the same colors than in Fig. 10a. The critical mutation rates involving the entrance into error threshold is displayed in red. The yellow arrows indicate the entrance into lethal mutagenesis. This plot has been built using $(p_0(0) = 0.1, n_0(0) = 0, p_1(0) = 0, n_1(0) = 0)$ as initial conditions. The same results are obtained with initial conditions (1, 0, 0, 0). Notice that lethal mutagenesis is replaced by the error catastrophe as α increases. (For interpretation of the references to color in this figure legend, the reader is referred to the web version of this article.)

Fig. 7 summarizes the bifurcations found in Eqs. (1)–(4) obtained by choosing different values of k_1 and tuning α from the SMR to the GR model. Here, for completeness, we overlap the information on stability for the origin, $\mathcal{O}$, displayed in Fig. 6. Several phase portraits are displayed for each case. The panel in Fig. 7a shows the orbits for $\sqrt{\alpha} = 0.85$ in the subspace (p_0, n_0), close to the GR

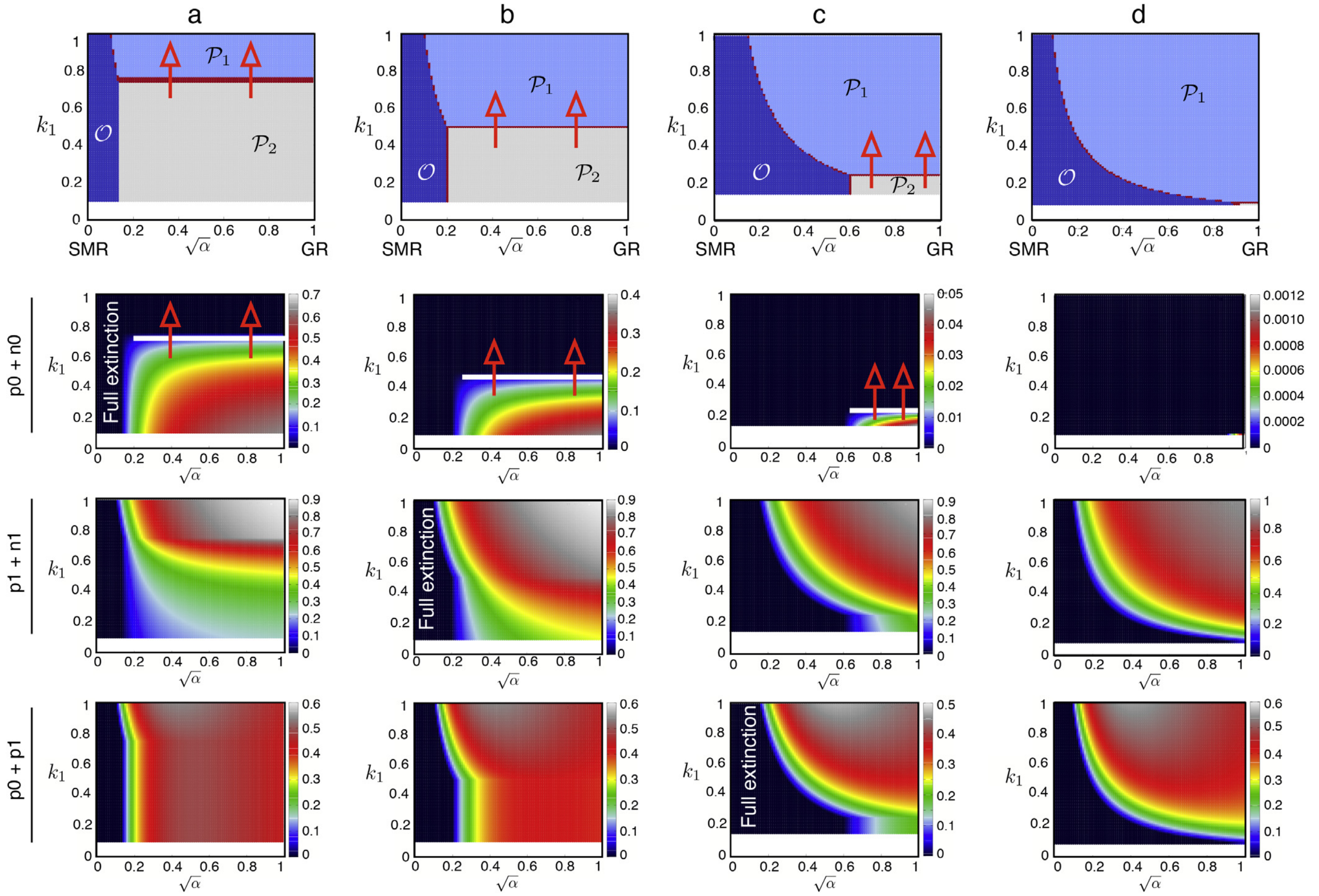

Fig. 10. Phase diagrams for the deleterious-neutral case displayed in Fig. 10a. We display the asymptotic dynamics in the parameter space $(\sqrt{\alpha}, k_1)$, with (a) $\mu = 0.25$ and $\varepsilon = 0.1$; (b) $\mu = 0.5$ and $\varepsilon = 0.1$; (c) $\mu = 0.75$ and $\varepsilon = 0.15$; (d) $\mu = 0.9$ and $\varepsilon = 0.09$. Legend: origin $\mathcal{O}$ (dark blue); $\mathcal{P}_1$ (light-blue); $\mathcal{P}_2$ (light-grey); and "no convergence" (dark red). Below the phase diagrams we display the equilibrium populations obtained numerically for variables: $p_0 + n_0$ (upper row); $p_1 + n_1$ (mid row); and $p_0 + p_1$ (lower row) $\mathcal{O}$. The horizontal white lines in the upper row display those critical values k_1 involving the dominance of the mutant sequences. (For interpretation of the references to color in this figure legend, the reader is referred to the web version of this article.)

mode. Here the attractor is $\mathcal{P}_2$, which involves the coexistence between master and mutant genomes. For the case $k_1 = 1 - \mu$ and for $\sqrt{\alpha} = 0.5$ the attractor achieved is $\mathcal{P}_1$, indicating that the population is dominated by the pool of mutants at equilibrium (Fig. 7b). The same asymptotic dynamics is found in the phase portrait of Fig. 7c. Finally, for $k_1 = 0$ we plot a case for which $\mathcal{P}_2$ is also locally asymptotically stable, while $\mathcal{O}$ is unstable (Fig. 7d).

Let us now focus our attention on the bifurcation diagram for the deleterious-neutral case. In this context, for a given value $0 < \mu < 1$ we consider a plane in the parameters $\sqrt{\alpha}$ and k_1. By hypothesis (H2), the diagram is restricted to the rectangle $(\sqrt{\alpha}, k_1) \in [0, 1] \times [\varepsilon, 1]$. The bifurcation curves $\sqrt{\alpha} = \nu_1$ and $\sqrt{\alpha} = \nu_0$ are, respectively, the hyperbola $\sqrt{\alpha}k_1 = \varepsilon$ and the vertical line $\sqrt{\alpha} = \varepsilon/(1 - \mu)$. The three colored areas in Fig. 8a correspond to the ω-limit (i.e., steady state achieved in forward time) of the solution starting with initial conditions $p_0(0) = 1,\ n_0(0) = p_1(0) = n_1(0) = 0$ (the same result hold with $p_0(0) = 0.1,\ n_0(0) = p_1(0) = n_1(0) = 0$). Namely, convergence to the origin $\mathcal{O}$ (red area); convergence to the equilibrium point $\mathcal{P}_1$ (light green area); attraction by the equilibrium point $\mathcal{P}_2$ (blue area). Observe that, when crossing these two bifurcation curves the equilibrium points change stability - by means of a transcritical bifurcation - or change the dimension of its associated local unstable invariant manifold (when they are saddles).

Similarly, we can plot a bifurcation diagram in the lethal case ($k_1 = 0$, Fig. 8b), now depending on the parameters $(\sqrt{\alpha}, 1 - \mu)$. Again, hypothesis (H2) implies that it takes places in the rectangle $[0, 1] \times [\varepsilon, 1]$. The bifurcation curve $\sqrt{\alpha} = \nu_0$ becomes a branch of the hyperbola $\sqrt{\alpha}(1 - \mu) = \varepsilon$. This curve also divides the domain in two coloured areas: a blue one, at the left-hand side of the hyperbola, characterized by the fact that the equilibrium point $\mathcal{O}$, the origin, is the ω-limit of the solution starting at the initial conditions $p_0(0) = 1,\ n_0(0) = p_1(0) = n_1(0) = 0$; an orange one, located on the right-hand side of the hyperbola, where the equilibrium point $\mathcal{P}_2^0$ is this ω-limit. Fig. 9 displays the regions in the parameter space $(\sqrt{\alpha}, \mu)$ where the different asymptotic states (obtained numerically) can be found for the deleterious-neutral cases: sequences extinction (red); dominance of mutant sequences (green); and coexistence of sequences (blue). Notice that these regions obtained numerically perfectly match with the analytical results derived in the article. In this plot we can identify the critical mutation values causing lethal mutagenesis (yellow arrows in Fig. 9), which occurs for $\sqrt{\alpha} < \varepsilon/k_1$. Above this threshold, lethal mutagenesis is replaced by the error catastrophe (red line in Fig. 9), with a critical mutation rate not depending on α. Notice that when the replication mode is close to the SMR lethal mutagenesis is achieved for lower mutation rates. This means that replication modes departing from the SMR provide the sequences with more resistance to lethal mutagenesis.

Finally, in Fig. 10 we display the basins of attraction of the fixed points for the neutral and deleterious mutants displayed in Fig. 8a. The red arrows indicate those values of k_1 responsible for the dominance of the mutant sequences (first and second rows in Fig. 10). Also, we numerically computed the relative populations for the master genomes (second row in Fig. 10), as well as of the mutants (third row) and the master and mutant (+) sense sequences.

6. Conclusions

The evolutionary dynamics of RNA viruses has been largely investigated seeking for critical thresholds involving error catastrophes and lethal mutagenesis (Manrubia and Lázaro, 2010; Pastor-Satorras and Solé, 2001; Solé et al., 2006). Typically, the so-called error catastrophe has been investigated using differential equations model, thus assuming continuous populations (Eigen, 1971; Manrubia and Lázaro, 2010). The error catastrophe and lethal mutagenesis concepts are rather different. Error catastrophe is an evolutionary shift in sequence space (Bull and Wilke, 2007), typically causing the outcompetition of the nonmutated master sequence by the cloud of mutants. Lethal mutagenesis has been described as a demographic process whereby viruses achieve extinctions due to a large accumulation of mutants of low fitness that reduce the effective population size thus making stochastic extinction events more likely (Bull and Wilke, 2007). This process was suggested by Loeb et al. (1999) as the mechanism behind the abolishment of viral replication for HIV-1 during *in vitro* mutagenic experiments. Further evidence on lethal mutagenesis in eukaryotic viruses have been found in lymphocytic choriomeningitis virus (Grande-Pérez et al., 2002) or influenza A virus (Pauley and Lauring, 2015). Recently, evidence for lethal mutagenesis *in vivo* have been reported for a plant virus (Díaz-Martínez et al., 2018).

Previous research on viral RNA replication modes has focused on theoretical and computational studies aiming at describing the evolutionary outcome of RNA sequences under the SMR and GR modes of replication. Smooth transitions have been identified in models for viral replication (Bull and Lachmann, 2005; Sardanyés et al., 2009). For instance, a simple model considering (+) and (−) sense genomes under differential replication modes identified a transcritical bifurcation (Sardanyés et al., 2012). This model, however, did not consider evolution. In this article we have studied a simple model considering both (+) and (−) sense sequences with differential replication modes evolving on a single-peak fitness landscape. Despite the simplicity of this landscape, being highly unrealistic, it has been used in multiple models as a simple approach to the dynamics of RNA viruses (Bull and Lachmann, 2005; Pastor-Satorras and Solé, 2001; Solé et al., 2006).

The model studied here has allowed us to derive the critical mutation values involving error thresholds and lethal mutagenesis considering three different types of mutant spectra, given by neutral, deleterious, and lethal mutants. We must note that lethal mutagenesis has been described as a demographic extinction (i.e., due to finite population effects) (Bull and Wilke, 2007). Here we provide an analogous mechanism for continuous populations (see below).

In the deleterious case, there are three possible scenarios when increasing the value of μ (we omit the trivial total extinction solution which is always assumed as a possible equilibrium): if $0 < k_1\sqrt{\alpha} < \varepsilon$, that is, close to the SMR mode, there is no nontrivial equilibrium solution. This happens for any $\mu > 0$. In the region of parameters $\varepsilon < \sqrt{\alpha} < \varepsilon/k_1$, between the SMR and GR modes (depending on the particular values of ε and k_1), the bifurcation undergone by the equilibria is quite steep. It passes from a situation with coexistence equilibrium to total extinction equilibrium when crossing the curve $\mu = \mu_c = 1 - (\varepsilon/\sqrt{\alpha})$. For $\varepsilon/k_1 < \sqrt{\alpha} < 1$, which always includes the GR case. When increasing μ, the systems shifts from coexistence to master sequences' extinction when crossing the critical value $\mu = 1 - k_1$.

Summarizing, the error threshold is achieved when the mutation rate is above the critical value μ_c, in the deleterious case is given by $\mu_c = 1 - \frac{\varepsilon}{\sqrt{\alpha}}$ if $\varepsilon < \sqrt{\alpha} < \frac{\varepsilon}{k_1}$; and $\mu_c = 1 - k_1$ if $\frac{\varepsilon}{k_1} < \sqrt{\alpha} < 1$. In the lethal case, there are only two scenarios: for $0 < \sqrt{\alpha} < \varepsilon$ (that is, almost pure SMR-mode), there are no nontrivial equilibria. For the rest of the cases, that is, $\varepsilon < \sqrt{\alpha} < 1$ the possible equilibrium solution goes from coexistence to total extinction.

Our results have allowed us to relate the processes of lethal mutagenesis and error catastrophe for continuous populations of viral genomes. Typically, these two different processes, suggested to impair viral persistence (Bull and Lachmann, 2005; Bull and Wilke, 2007; Loeb et al., 1999; Manrubia and Lázaro, 2010), have been treated separately. Our model establishes the parametric conditions allowing theoretical viral quasispecies to shift from one process to the other taking into account different replication modes.

Acknowledgements

The research leading to these results has received funding from “la Caixa” Foundation and from a Ministerio de Economia y Competitividad grant awarded to the Barcelona Graduate School of Mathematics (BGSMath) under the “María de Maeztu” Program (grant MDM-2014-0445). JS has been also funded by a Ramón y Cajal Fellowship (RYC-2017-22243). JS and TA have been partially funded by the CERCA Programme of the Generalitat de Catalunya. JTL has been partially supported by the MINECO/FEDER grant MTM2015-65715-P, by the Catalan grant 2014SGR-504 and by the Russian Scientific Foundation grants 14-41-00044 and 14-12-00811. TA is also supported by the AGAUR (grant 2014SGR-1307) and the MINECO (grant MTM2015-71509-C2-1-R). SFE has been supported by MINECO-FEDER grant BFU2015-65037-P and by Generalitat Valenciana grant PROMETEOII/2014/021.

Appendix A. Proof of Proposition 1

Let us deal, first, with the deleterious case ($0 < k_1 < 1$). In this framework, equilibrium states will come from the solutions of the following system of non-linear equations:

$$(1-\mu)n_0\phi = \varepsilon p_0, \tag{10}$$

$$\alpha(1-\mu)p_0\phi = \varepsilon n_0, \tag{11}$$

$$(\mu n_0 + k_1 n_1)\phi = \varepsilon p_1, \tag{12}$$

$$\alpha(\mu p_0 + k_1 p_1)\phi = \varepsilon n_1. \tag{13}$$

It is clear that the origin $\mathcal{O}$ is a fixed point of our system in all the cases. To find nontrivial solutions we distinguish three different scenarios for these equilibria: (i) master sequences extinction; (ii) mutant sequences extinction and (iii) coexistence among all sequences.

(i) Case $p_0 = n_0 = 0$ (master sequences extinction): If we assume $p_1 = 0$, substituting in Eq. (13) and using that $\varepsilon \neq 0$, we get $n_1 = 0$ and therefore, the equilibrium is $\mathcal{O} = (0, 0, 0, 0)$, the trivial solution. A symmetric situation undergoes when we start taking $n_1 = 0$.

Thus, let us assume that $p_1 \neq 0$ and $n_1 \neq 0$. Replacing $p_0 = n_0 = 0$ in (12)–(13) and dividing such equations we get $p_1/n_1 = n_1/(\alpha p_1)$ and so $n_1 = \sqrt{\alpha} p_1$. This division is well-defined since $p_1 > 0$, $k_1 > 0$ and $\phi \neq 0$ (if $\phi = 0$ it is straightforward to check that it leads to the origin $\mathcal{O}$ as fixed point). From Eq. (13) we obtain $\varepsilon\sqrt{\alpha} = \alpha k_1(1-\sqrt{\alpha}p_1 - p_1)$ and thus

$$\begin{aligned} p_1 &= p_1^* = \frac{1}{\sqrt{\alpha}(1+\sqrt{\alpha})}(\sqrt{\alpha} - \nu_1) \\ &= c_\alpha(\sqrt{\alpha} - \nu_1), \end{aligned}$$

where ν_1 and c_α have been defined in (5). Therefore, since $n_1 = \sqrt{\alpha}p_1$ we get the equilibrium point $\mathcal{P}_1 = p_1^*\big(0, 0, 1, \sqrt{\alpha}\big)$ provided $\sqrt{\alpha} > \nu_1$ (since we are interested in nontrivial equilibrium points with biological meaning).

(ii) Case $p_1 = n_1 = 0$ (mutant sequence extinction): in this scenario one has to solve

$$\begin{aligned} (1-\mu)n_0(1-p_0-n_0) &= \varepsilon p_0, \\ \alpha(1-\mu)p_0(1-p_0-n_0) &= \varepsilon n_0, \\ \mu n_0(1-p_0-n_0) &= 0, \\ \alpha\mu p_0(1-p_0-n_0) &= 0. \end{aligned}$$

As before, both cases $p_0 = 0$ and $n_0 = 0$ lead to the equilibrium point $\mathcal{O}$. So let us consider the case of $p_0 \neq 0$ and $n_0 \neq 0$. From the last two equations it follows that $p_0 + n_0 = 1$ and substituting in the two ones we get $p_0 = n_0 = 0$, which is a contradiction. So there is no nontrivial equilibrium points with $p_1 = n_1 = 0$.

(iii) Coexistence sequences equilibria: multiplying Eq. (11) by p_0 and subtracting Eq. (10) multiplied by n_0 it turns out that $(1-\mu)\phi(\alpha p_0^2 - n_0^2) = 0$. Since $0 < \mu < 1$, this leads to three possibilities, namely, (a) $\phi = 0$ (that is $p_0 + n_0 + p_1 + n_1 = 1$) or (b) $n_0 = \sqrt{\alpha}p_0$ with $\phi \neq 0$ and (c) $\phi = 0$ and $n_0 = \sqrt{\alpha}p_0$.

Case (c) does not apply. Indeed, substituting $\phi = 0$ and $n_0 = \sqrt{\alpha}p_0$ into Eq. (10) one gets that $p_0 = 0$ and so $n_0 = 0$, which is not possible. A similar argument shows that case (a) does not hold. In fact, taking $\phi = 0$ in equations (10)–(13) leads to $p_0 = n_0 = p_1 = n_1 = 0$ which contradicts $\phi = 0 \Leftrightarrow p_0 + n_0 + p_1 + n_1 = 1$. Thus, let us deal with case (b).

Substituting $n_0 = \sqrt{\alpha}p_0$ in (10) and using that $p_0 \neq 0$ (if $p_0 = 0 \Rightarrow n_0 = 0$, which corresponds to the master sequences extinction case) it turns out that

$$(1-\mu)\sqrt{\alpha}\phi = \varepsilon \Rightarrow \phi\sqrt{\alpha} = \frac{\varepsilon}{1-\mu} \Rightarrow \phi\sqrt{\alpha} = \nu_0.$$

It is straightforward to check that Eq. (11) leads to the same condition. Performing again the change $n_0 = \sqrt{\alpha}p_0$ onto equations (12) and (13) one gets

$$\begin{aligned} \mu\sqrt{\alpha}p_0\phi + k_1 n_1\phi &= \varepsilon p_1, \\ \alpha\mu p_0\phi + \alpha k_1 p_1\phi &= \varepsilon n_1. \end{aligned} \tag{14}$$

Computing the division between Eq. (12) and (13), namely,

$$\begin{aligned} &\frac{\mu\sqrt{\alpha}p_0 + k_1 n_1}{\alpha(\mu p_0 + k_1 p_1)} = \frac{p_1}{n_1} \\ &\Rightarrow \mu\sqrt{\alpha}p_0 n_1 + k_1 n_1^2 = p_1\alpha(\mu p_0 + k_1 p_1) \\ &\Rightarrow \mu p_0\sqrt{\alpha}(n_1 - \sqrt{\alpha}p_1) = k_1(\alpha p_1^2 - n_1^2), \end{aligned}$$

one gets

$$\begin{aligned} &\mu p_0\sqrt{\alpha}(n_1 - \sqrt{\alpha}p_1) \\ &= -k_1(n_1 - \sqrt{\alpha}p_1)(\sqrt{\alpha}p_1 + n_1). \end{aligned}$$

So now we have two possibilities: $n_1 = \sqrt{\alpha}p_1$ or $n_1 \neq \sqrt{\alpha}p_1$. Observe that the latter cannot be since in that case we would have that $p_0 = -\frac{k_1}{\mu\sqrt{\alpha}}(n_1 - \sqrt{\alpha}p_1) < 0$, which is not possible because p_0 is positive. Therefore, it must be $n_1 = \sqrt{\alpha}p_1$. Substituting it into (14) we have $\mu p_0\nu_0 + k_1 p_1\nu_0 = \varepsilon p_1$, which implies

$$\mu p_0 + \left(k_1 - \frac{\varepsilon}{\nu_0}\right)p_1 = 0.$$

Notice that $k_1 - (\varepsilon/\nu_0) = 0 \Leftrightarrow \nu_0 = \nu_1$. In fact, we have that $\nu_0 \neq \nu_1$. Indeed, if this term vanished we would have $p_0 = 0$ and thus $n_0 = 0$, which gives rise to point $\mathcal{P}_1$.

Hence, if $k_1 - (\varepsilon/\nu_0) \neq 0$, it follows that

$$\begin{aligned} p_1 &= \frac{\mu}{\frac{\varepsilon}{\nu_0} - k_1}p_0 \\ &= \frac{\mu\nu_0}{\varepsilon - k_1\nu_0}p_0 = \frac{\mu\nu_0}{k_1(\nu_1 - \nu_0)}p_0 = \delta p_0. \end{aligned} \tag{15}$$

Thus, $\phi = 1 - (p_0 + n_0 + p_1 + n_1) = 1 - (1+\sqrt{\alpha})p_0 - (1+\sqrt{\alpha})p_1$ and so

$$p_0 + p_1 = c_\alpha(\sqrt{\alpha} - \nu_0)$$

Combining the previous relation with (15) the following solution is obtained

$$\begin{aligned} p_0 &= q_0 = \frac{c_\alpha(\sqrt{\alpha} - \nu_0)}{1+\delta}, \\ n_0 &= \sqrt{\alpha}q_0, \\ p_1 &= \delta q_0, \\ n_1 &= \delta\sqrt{\alpha}q_0, \end{aligned}$$

with ν_0, c_α, δ defined in (5)–(6), which leads to the coexistence equilibrium state

$$\mathcal{P}_2 = q_0\big(1, \sqrt{\alpha}, \delta, \delta\sqrt{\alpha}\big),$$

for $\sqrt{\alpha} > \nu_0$ and $\nu_0 < \nu_1$.

Concerning the neutral case ($k_1 = 1$), it is easy to check that all the computations carried out for the deleterious context are also valid for this case.

And the last, but not least, case corresponds to the lethal framework ($k_1 = 0$). Equilibrium states must be solution of the system

$$(1-\mu)n_0\phi - \varepsilon p_0 = 0, \tag{16}$$

$$\alpha(1-\mu)p_0\phi - \varepsilon n_0 = 0, \tag{17}$$

$$\mu n_0\phi - \varepsilon p_1 = 0, \tag{18}$$

$$\alpha\mu p_0\phi - \varepsilon n_1 = 0. \tag{19}$$

Again, the origin $\mathcal{O}$ is a trivial fixed point. To seek for nontrivial equilibria we take into account two scenarios: (a) $p_0 = 0$; (b) $p_0 \neq 0$.

(a) Case $p_0 = 0$: From the equation (16) we get $(1-\mu)n_0\phi = 0$. Since $0 < \mu < 1$ we have three possibilities: $n_0 = 0$, $\phi = 0$ or both. It is obvious that first and third cases lead to the origin $\mathcal{O}$. Regarding to the case with $\phi = 0$, it follows that $n_0 + n_1 + p_1 = 1$. Substituting it into equations (17)–(19) we get $n_0 = p_1 = n_1 = 0$, which contradicts the previous equality.

(b) Case $p_0 \neq 0$: From (16) we have that neither n_0 nor ϕ vanish. Performing $n_0 \times$ (16) minus $p_0 \times$ (17) one gets that $(1-\mu)\phi(n_0^2 - \alpha p_0^2) = 0$ and so $n_0 = \sqrt{\alpha}p_0$ since $0 < \mu < 1$ and $\phi \neq 0$. Substituting the latter equality into (16) it follows that $(1-\mu)\sqrt{\alpha}\phi = \varepsilon \Rightarrow \sqrt{\alpha}\phi = \nu_0$.

Subtracting $n_0 \times$ (19) from $\alpha p_0 \times$ (18) one has $\varepsilon p_0\sqrt{\alpha}(\sqrt{\alpha}p_1 - n_1) = 0$, so then $n_1 = \sqrt{\alpha}p_1$. On the other hand,

$$\begin{aligned} \sqrt{\alpha}\phi &= \nu_0 \Rightarrow 1 - (1+\sqrt{\alpha})(p_0 + p_1) \\ &= \frac{\nu_0}{\sqrt{\alpha}} \Rightarrow p_0 + p_1 = \frac{\sqrt{\alpha} - \nu_0}{\sqrt{\alpha}(1+\sqrt{\alpha}} \\ &= c_\alpha(\sqrt{\alpha} - \nu_0). \end{aligned}$$

And last, from (19) and using that $\sqrt{\alpha}\phi = \nu_0$ and $n_1 = \sqrt{\alpha}p_1$ we get $\alpha\mu p_0\phi = \varepsilon n_1 \Rightarrow p_1 = \delta^0 p_0$. Therefore the equilibrium point is given by

$$\mathcal{P}_2^0 = q_0^0\left(1, \sqrt{\alpha}, \delta, \delta\sqrt{\alpha}\right),$$

where $q_0^0 = c_\alpha(\sqrt{\alpha} - \nu_0)/(1+\delta^0)$ and provided that $\sqrt{\alpha} > \nu_0$ (to have biological meaning).

Appendix B. Proof of Proposition 2

As mentioned before, the case $\mu = 1$ corresponds to the situation where the master sequence mutates with probability 1. Thus, concerning their equilibrium points we have:

- In the deleterious and neutral cases, substituting $\mu = 1$ into Eqs. (10)–(13), one gets the equations

  $$\begin{aligned} &\varepsilon_0 p_0 = 0, \quad \varepsilon n_0 = 0,\\ &(n_0 + k_1 n_1)\phi = \varepsilon p_1,\\ &\alpha(p_0 + k_1 p_1)\phi = \varepsilon n_1. \end{aligned}$$

  From the two first equations it follows that $p_0 = n_0 = 0$ and, consequently

  $$k_1 n_1 \phi = \varepsilon p_1, \qquad \alpha k_1 p_1 \phi = \varepsilon n_1. \tag{20}$$

  Again, we distinguish several possibilities:
  - If $n_1 = 0$ then $p_1 = 0$ and so we obtain the origin.
  - If $p_1 = 0$ then $n_1 = 0$ and therefore the equilibrium point is again the origin.
  - In case that $n_1 + p_1 = 1$, $n_1 \neq 0$, $p_1 \neq 0$ it follows that $\phi = 0$ and so $p_1 = n_1 = 0$ which is a contradiction with the fact that $n_1 + p_1 = 1$.
  - Finally, if $n_1 \neq 0$, $p_1 \neq 0$, $\phi \neq 0$, we can divide them and get $\alpha p_1/n_1 = n_1/p_1$. Consequently, $n_1 = \sqrt{\alpha}p_1$. This gives rise to an equilibrium of the form $(0, 0, p_1, \sqrt{\alpha}p_1)$. Substituting this form into the first equation of (20), one obtains $p_1 = c_\alpha(\sqrt{\alpha} - \nu_1)$, defined provided $\sqrt{\alpha} > \nu_1$, which corresponds to the point $\mathcal{P}_1$ in Proposition 1.
- In the lethal case, equilibria system (16)–(19) reduces to $\varepsilon p_0 = 0$, $\varepsilon n_0 = 0$, $n_0\phi = \varepsilon p_1$, $\alpha p_0 \phi = \varepsilon n_1$. From the first two equations we have $p_0 = n_0 = 0$ and substituting in the second ones, it turns out $p_1 = n_1 = 0$, that is, the origin.

Appendix C. Proof of Proposition 3

As usual, we use stability analysis of the linearised system around the equilibrium to determine, when possible, the local nonlinear stability of the point for the complete system.

1. Deleterious and neutral case ($0 < k_1 \leq 1$): the eigenvalues of the differential matrix

   $$A_{\mathcal{O}} = DF(\mathcal{O}) = \begin{pmatrix} -\varepsilon & 1-\mu & 0 & 0 \\ \alpha(1-\mu) & -\varepsilon & 0 & 0 \\ 0 & \mu & -\varepsilon & k_1 \\ \alpha\mu & 0 & \alpha k_1 & -\varepsilon \end{pmatrix},$$

   are $\lambda_1 = -\varepsilon + \sqrt{\alpha}(1-\mu)$, $\lambda_2 = -\varepsilon - \sqrt{\alpha}(1-\mu)$, $\lambda_3 = -\varepsilon + k_1\sqrt{\alpha}$, and $\lambda_4 = -\varepsilon - k_1\sqrt{\alpha}$. It is easy to verify that $v_3 = \mathcal{O}\mathcal{P}_1 = (0, 0, 1, \sqrt{\alpha})$ and $v_4 = (0, 0, -1, \sqrt{\alpha})$ are eigenvectors of λ_3 and λ_4, respectively. It is also straightforward to check that

   $$\begin{cases} \lambda_1 < 0 & \text{if } \sqrt{\alpha} < \nu_0, \\ \lambda_1 = 0 & \text{if } \sqrt{\alpha} = \nu_0, \\ \lambda_1 > 0 & \text{if } \sqrt{\alpha} > \nu_0, \end{cases}$$

   and

   $$\begin{cases} \lambda_3 < 0 & \text{if } \sqrt{\alpha} < \nu_1, \\ \lambda_3 = 0 & \text{if } \sqrt{\alpha} = \nu_1, \\ \lambda_3 > 0 & \text{if } \sqrt{\alpha} > \nu_1. \end{cases}$$

   Thus, we have the following three cases:
   - Case $0 < k_1 < 1 - \mu$ or, equivalently, $\nu_0 < \nu_1$: the origin is a sink (an attractor) for $\alpha \in (0, \nu_0)$ and unstable (saddle) for $\sqrt{\alpha} \in (\nu_0, 1)$. For $\alpha \in (\nu_0, \nu_1)$ one has $\dim W^u_{\text{loc}}(\mathcal{O}) = 1$ and if $\sqrt{\alpha} > \nu_1$ then $\dim W^u_{\text{loc}}(\mathcal{O}) = 2$.
   - Case $k_1 = 1 - \mu$ or, equivalently, $\nu_0 = \nu_1$: the origin is a sink for $\sqrt{\alpha} \in (0, \nu_0)$ and unstable (saddle) for $\sqrt{\alpha} \in (\nu_0, 1)$. The dimension of $W^u_{\text{loc}}(\mathcal{O})$ is 2 in this interval.
   - Case $1 - \mu < k_1 < 1$ or, equivalently, $\nu_1 > \nu_0$: the origin is a sink if $\sqrt{\alpha} < \nu_1$ and unstable (a saddle) for $\sqrt{\alpha} > \nu_1$. The dimension $\dim W^u_{\text{loc}}(\mathcal{O})$ goes from 1 to 2 when $\sqrt{\alpha}$ crosses ν_0.
2. Lethal case ($k_1 = 0$): The eigenvalues of

   $$A_{\mathcal{O}} = DF(0, 0, 0, 0) = \begin{pmatrix} -\varepsilon & 1-\mu & 0 & 0 \\ \alpha(1-\mu) & -\varepsilon & 0 & 0 \\ 0 & \mu & -\varepsilon & 0 \\ \alpha\mu & 0 & 0 & -\varepsilon \end{pmatrix}$$

   are in this case

   $$\begin{aligned} \lambda_1 &= -\varepsilon + \sqrt{\alpha}(1-\mu), \\ \lambda_2 &= -\varepsilon - \sqrt{\alpha}(1-\mu), \\ \lambda_3 &= -\varepsilon, \\ \lambda_4 &= -\varepsilon. \end{aligned}$$

   Observe that $\lambda_2 < 0$, $\lambda_3 < 0$ and $\lambda_4 < 0$ so the stability of $\mathcal{O}$ depends only on λ_1. Indeed:

   $$\begin{cases} \lambda_1 < 0 & \text{if } \sqrt{\alpha} < \nu_0, \\ \lambda_1 = 0 & \text{if } \sqrt{\alpha} = \nu_0, \\ \lambda_1 > 0 & \text{if } \sqrt{\alpha} > \nu_0. \end{cases}$$

   Therefore, the origin is asymptotically stable for $\sqrt{\alpha} < \nu_0$ and becomes unstable for $\sqrt{\alpha} > \nu_0$. This situation is represented in Fig. 6.

Appendix D. Proof of Proposition 5

Recall that $\sqrt{\alpha} > \nu_0$ since $\mathcal{P}_2$ exists. We distinguish two cases:

1. Case 1: deleterious mutants ($0 < k_1 < 1$) with $0 < k_1 < 1 - \mu$ (that is, equivalently, $\nu_0 < \nu_1$). The expression of the eigenvalues can directly from algebraic computations. They are all real. Observe that λ_1, λ_2 and λ_+ are negative. Concerning λ_-, notice that

   $$\begin{aligned} &|A - 2((1-\mu) - k_1)\varepsilon| < A \\ &\Leftrightarrow 0 < A - ((1-\mu) - k_1)\varepsilon < A. \end{aligned}$$

   The second inequality is trivially satisfied since $(1-\mu) - k_1 > 0$ and $\varepsilon > 0$. Regarding the first one, one can check that

   $$\begin{aligned} &0 < A - ((1-\mu) - k_1) \\ &\Leftrightarrow \sqrt{\alpha}(1-\mu)^2 - k_1\varepsilon > (1-\mu)\varepsilon - k_1\varepsilon \\ &\Leftrightarrow \sqrt{\alpha} > \nu_0, \end{aligned}$$

   which is satisfied by hypothesis. Therefore, $A - |A - 2((1-\mu) - k_1)\varepsilon| > 0$ and, consequently, $\lambda_- < 0$. This implies that the point $\mathcal{P}_2$ is a sink for any $\sqrt{\alpha} > \nu_0$.
2. Case 2: lethal mutants ($k_1 = 0$). As above, the expression for the eigenvalues follows from linear algebra and straightforward computations. Again, λ_1, λ_2, and λ_- are all three real and negatives. Concerning λ_+ (real), we define $B = (1-\mu)\sqrt{\alpha}/2$. This implies that $\lambda_+ = -B + |B - \varepsilon|$. Observe that $|B - \varepsilon| < B \Leftrightarrow 0 < 2B - \varepsilon$. Right-hand inequality is trivial since $\varepsilon > 0$. Left-hand is also satisfied since it is equivalent to $\sqrt{\alpha} > \nu_0$. So, all four eigenvalues are real and negative which means that the point $\mathcal{P}_2^0$ is a sink for any $\sqrt{\alpha} > \nu_0$.

References

Bull, J.J., Meyers, L.A., Lachmann, M., 2005. Quasispecies made simple. PLoS Comput. Biol 1 (6), e61.

Bull, J.J., Sanjuán, R., Wilke, C.O., 2007. Theory of lethal mutagenesis for viruses. J. Virol. 81 (6), 2930–2939.

Carrasco, P., de la Iglesia, F., Elena, S.F., 2007. Distribution of fitness and virulence effects caused by single-nucleotide substitutions in tobacco etch virus. J. Virol. 81, 12979–12984.

Chao, L., Rang, C.U., Wong, L.E., 2002. Distribution of spontaneous mutants and inferences about the replication mode of the RNA bacteriophage ϕ6. J. Virol. 76, 3276–3281.

Combe, M., Garijo, R., Geller, R., Cuevas, J.M., Sanjuán, R., 2018. Single-cell analysis of RNA virus infection identifies multiple genetically diverse viral genomes within single infectious units. Cell Host Microbe 18, 424–432.

Díaz-Martínez, L., Brichette-Mieg, I., Domínguez-Huerta, G., Grande-Pérez, A., 2018. Lethal mutagenesis of an RNA plant virus via lethal defection. Sci. Rep. 8, 1444.

Eigen, M., 1971. Self organization of matter and the evolution of biological macromolecules. Naturwissenschaften 58 (10), 465–523. doi:10.1007/BF00623322.

Elena, S.F., Carrasco, P., Daròs, J.A., Sanjuán, R., 2006. Mechanisms of genetic robustness in RNA viruses. EMBO Rep. 7, 168–173.

Garcia-Villada, L., Drake, J.W., 2012. The three faces of riboviral spontaneous mutation: spectrum, mode of genome replication, and mutation rate. PLoS Genet. 8, e1002832.

Grande-Pérez, A., Sierra, S., Castro, M.G., Domingo, E., Lowenstein, P.R., 2002. Molecular indetermination in the transition to error catastrophe: systematic elimination of lymphocytic choriomeningitis virus through mutagenesis does not correlate linearly with large increases in mutant spectrum complexity. Proc Natl Acad Sci USA 99, 12938–12943.

Hutchison, C.A.I., Sinsheimer, R.L., 1966. The process of infection with bacteriophage ϕx174. x. mutations in a ϕx lysis gene. J. Mol. Biol. 18, 429–447.

Lalic, J., Elena, S.F., 2015. The impact of high-order epistasis in the within-host fitness of a positive-sense plant RNA virus. J. Evol. Biol. 28, 2236–2247.

Loeb, L.A., Essigmann, J.M., Rose, K.D., Kazazi, F., Mullins, J.I., 1999. Lethal mutagenesis of HIV with mutagenic nucleoside analogs. Proc. Natl. Acad. Sci. USA. 96, 1492–1497.

Luria, S., 1951. The frequency distribution of spontaneous bacteriophage mutants as evidence for the exponential rate of phage reproduction. Cold Spring Harbor Symp. Quant. Biol. 16, 463–470.

Luria, S., Delbrück, M., 1943. Mutations of bacteria from virus sensitivity to virus resistance. Genetics 28, 491–511.

Manrubia, S.C., Domingo, E., Lázaro, E., 2010. Pathways to extinction: beyond the error threshold. Philos. Trans. R. Soc. Lond. B 365, 1943–1952.

Martínez, F., Sardanyès, J., Elena, S.F., Daròs, J.A., 2011. Dynamics of a plant RNA virus intracellular accumulation: stamping machine vs. geometric replication. Genetics 188, 637–646.

Pastor-Satorras, R., Solé, R.V., 2001. Field theory for a reaction-diffusion model of quasispecies dynamics. Phys. Rev. E 64 (5), 051909.

Pauley, M.D., Lauring, A.S., 2015. Effective lethal mutagenesis of influenza virus by three nucleoside analogs. J. Virol. 89, 3584–3597.

Sanjuán, R., Nebot, M.R., Chirico, N., Mansky, L.M., Belshaw, R., 2010. Viral mutation rates. J. Virol. 84, 9733–9748.

Sanjuán, R., Domingo-Calap, P., 2016. Mechanisms of viral mutation. Cell Mol. Life Sci. 73. 4433–3338

Sanjuán, R., Moya, A., Elena, S.F., 2004. The distribution of fitness effects caused by single-nucleotide substitutions in an RNA virus. Proc. Natl. Acad. Sci. U.S.A. 101, 8396–8401.

Sardanyés, F., Martínez, J., Daròs, J.A., Elena, S.F., 2012. Dynamics of alternative modes of RNA replication for positive-sense RNA viruses. J. Roy. Soc. Interface 11, 768–776.

Sardanyés, J., Elena, S.F., 2011. Quasispecies spatial models for RNA viruses with different replication modes and infection strategies. PloS one 6 (9), e24884.

Sardanyés, J., Solé, R.V., Elena, S.F., 2009. Replication mode and landscape topology differentially affect RNA virus mutational load and robustness.. J. Virol. 83 (23), 12579–12589.

Schulte, M.B., Draghi, J.A., Plotkin, J.B., Andino, R., 2015. Experimentally guided models reveal replication principles that shape the mutation distribution of RNA viruses. eLife 4, e03753.

Solé, R.V., Sardanyés, J., Díez, J., Mas, A., 2006. Information catastrophe in RNA viruses through replication thresholds. J. Theor. Biol. 240 (3), 353–359.

Stent, G., 1963. Molecular Biology of Bacterial Viruses. San Francisco, CA: W H Freeman and Company.

Swetina, J., Schuster, P., 1982. Self-replication with errors. a model for polynucleotide replication. Biophys. Chem. 16, 329–345.